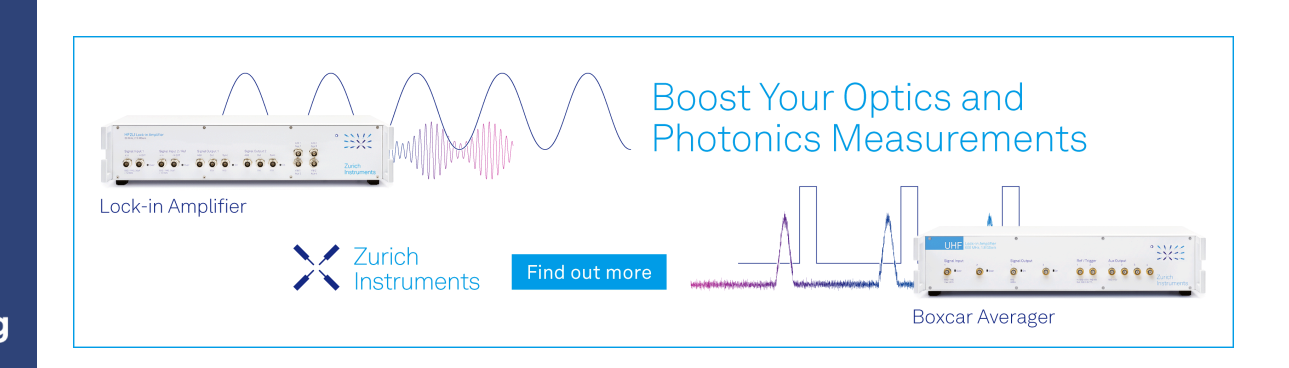
# A model of heterogeneous undercooled liquid and glass accounting for temperature-dependent nonexponentiality and enthalpy fluctuation [REE]











### A model of heterogeneous undercooled liquid and glass accounting for temperature-dependent nonexponentiality and enthalpy fluctuation

Cite as: J. Chem. Phys. 160, 174504 (2024); doi: 10.1063/5.0196812 Submitted: 9 January 2024 • Accepted: 15 April 2024 • Published Online: 2 May 2024







Wataru Takeda (D) and Pierre Lucas (D)





### **AFFILIATIONS**

Department of Materials Science and Engineering, University of Arizona, Tucson, Arizona 85712, USA

a) Author to whom correspondence should be addressed: pierre@arizona.edu

### **ABSTRACT**

Dynamic heterogeneity is a fundamental characteristic of glasses and undercooled liquids. The heterogeneous nature causes some of the key features of systems' dynamics such as the temperature dependence of nonexponentiality and spatial enthalpy fluctuations. Commonly used phenomenological models such as Tool-Narayanaswamy-Moynihan (TNM) and Kovacs-Aklonis-Hutchinson-Ramos fail to fully capture this phenomenon. Here we propose a model that can predict the temperature-dependent nonexponential behavior observed in glass-forming liquids and glasses by fitting standard differential scanning calorimetry curves. This model extends the TNM framework of structural relaxation by introducing a distribution of equilibrium fictive temperature ( $T_i^e$ ) that accounts for heterogeneity in the undercooled liquid. This distribution is then frozen at the glass transition to account for the heterogeneous nature of the glass dynamics. The nonexponentiality parameter  $\beta_{KWW}$  is obtained as a function of temperature by fitting the Kohlrauch-Williams-Watts (KWW) equation to the calculated relaxation function for various organic and inorganic undercooled liquids and glasses. The calculated temperature dependent  $\beta_{\rm KWW}$  shows good agreement with the experimental ones. We successfully model the relaxation dynamics far from equilibrium for two silicate systems that the TNM model fails to describe, confirming that temperature dependent nonexponentiality is necessary to fully describe these dynamics. The model also simulates the fluctuation of fictive temperature  $\delta T_f$  during isothermal annealing with good qualitative agreement with the evolution of enthalpy fluctuation reported in the literature. We find that the evolution of enthalpy fluctuation during isothermal annealing heavily depends on the cooling rate, a dependence that was not previously emphasized.

Published under an exclusive license by AIP Publishing. https://doi.org/10.1063/5.0196812

#### I. INTRODUCTION

Glasses are ubiquitous in modern society, and their application spans from window glass, electronics, and photonics<sup>1,2</sup> to pharmaceuticals<sup>3</sup> and biomedical devices.<sup>4</sup> Despite their familiarity in our daily life, the prediction of glass dynamics such as "physical aging" and glass transition is challenging.<sup>5-7</sup> Physical aging refers to the property changes induced by structural rearrangement over time. A major challenge in predicting aging arises from complex structural dynamics that can be identified as having three "non" characteristics: (1) nonlinear, (2) non-Arrhenius, and (3) nonexponential.<sup>8</sup> The nonlinear relaxation of glasses is the consequence of their nonequilibrium nature and can be parametrized through the concept of fictive temperature. 9,10 Non-Arrhenius temperature dependence of the relaxation time of glass-forming liquids is a well-known phenomenon that can be parametrized by Angell's

fragility index.<sup>11</sup> Nonexponential relaxation can be parametrized by fitting relaxation data to the Kohlrausch-Williams-Watts (KWW) equation as<sup>11</sup>

$$\Psi(t) = \exp\left(-\left(\frac{t}{\tau_{\text{KWW}}}\right)^{\beta_{\text{KWW}}}\right),\tag{1}$$

where  $\Psi(t)$  is the relaxation function or correlation function, t is time,  $\tau_{KWW}$  is the characteristic relaxation time of a system, and  $\beta_{\rm KWW}$  is the nonexponentiality parameter. Many studies have shown that nonexponential relaxation originates from the spatially heterogeneous nature of glass. 14,15 Such spatial heterogeneity appears in undercooled liquids and grows as the glass transition approaches. Adam and Gibbs (AG) suggested that the growth of such regions' size is responsible for the dramatic increase in viscosity near the

glass transition. 16 Such a region is called a cooperatively rearranging region (CRR). There is no explicit definition of CRR in the theory of Adam and Gibbs (AG); therefore, researchers have evolved a similar quantity called the heterogeneity length scale  $(\xi)$ . Various experimental methods have been used to identify  $\xi_1^{17-20}$  and the growth of  $\xi$  near the glass transition has been observed by both experiments and simulations.<sup>21–23</sup> Theories like the random-firstorder transition (RFOT) theory<sup>24</sup> or hierarchical dynamic facilitation predict the growing length scale of  $\xi$ . According to Donth's fluctuation dissipation theorem (DFDT), the effect of this spatial heterogeneity can be probed through calorimetric experiments such as heat capacity spectroscopy (HCS) and temperature modulated differential scanning calorimetry (TMDSC) at the glass transition. 20,26,27 The DFDT uses thermodynamic fluctuation theory and introduces temperature fluctuations  $\delta T$  for the estimation of the volume of fluctuating regions,  $V_{\rm DFDT} \approx \xi^3$ .

When a glass is subjected to isothermal annealing below the glass transition, heterogeneity plays an important role.<sup>28</sup> Because some microdomains relax faster, the macroscopic structural evolution exhibits complex relaxation dynamics. This heterogeneous relaxation is the origin of nonexponential relaxation. For example, a complex thermal history affects the enthalpy recovery during isothermal annealing, as revealed by the nonmonotonic evolution of the refractive index observed by Macedo and Napolitano.<sup>29</sup> This behavior was explained and modeled by considering a distribution of relaxation times. It is known that the nonexponentiality parameter  $\beta_{\rm KWW}$  that reflects this distribution of relaxation times not only depends on the chemical composition of a system but also on temperature. 30-32 Specifically, the distribution of relaxation time becomes broader at lower temperatures. This has been observed experimentally by dielectric spectroscopy,<sup>33</sup> HCS, and electron correlation microscopic measurements.<sup>23</sup> The RFOT theory also predicts such a decrease in  $\beta_{\rm KWW}$  for both undercooled liquid and glass, and it is attributed to the broadening of activation barriers for the rearranging microscopic domains.<sup>34</sup> However, for some glass-forming liquids, evidence against this heterogeneous picture of nonexponential relaxation exists, and instead, homogeneous relaxation is invoked.3

A distribution of density/enthalpy domains in undercooled liquids and glasses has also been observed in both experiments and simulations. Light scattering experiments show an anomaly in density fluctuation in B<sub>2</sub>O<sub>3</sub> during reheating,<sup>38</sup> which was characterized and explained by Moynihan and Schroeder<sup>39</sup> and Lee *et al.*<sup>40</sup> The enthalpy landscape model developed by Mauro and Loucks shows a finite width in the distribution of density/enthalpy in both the undercooled equilibrium liquid state and the glassy state.<sup>41</sup> The model shows that the distribution of density in the glassy state evolves nonmonotonically during isothermal annealing below the glass transition, which was confirmed by an *in situ* small angle x-ray scattering (SAXS) experiment.<sup>42</sup>

Commonly used models such as the Tool–Narayanaswamy–Moynihan–Hodge (TNMH) model  $^{9,10,43,44}$  and the Kovacs–Aklonis–Hutchinson–Ramos (KAHR) model  $^{45,46}$  for glass dynamics phenomenologically account for the three "nons" mentioned earlier. They show excellent agreement with observations near  $T_{\rm g}$ . However, poor agreement in relaxation dynamics is found far from equilibrium.  $^{47,48}$  Possible explanations for these deviations may be the "single fictive temperature" approach to the glass

dynamics and the temperature-independent nonexponentiality. Previously, several attempts have been made to overcome this single fictive temperature approach.  $^{47,50}$  Such models introduce a local fictive temperature  $T_{f,i}$  with weights  $W_i (i=1,2,3,\ldots,N)$ . The evolution of these  $T_{f,i}$  is then computed during various thermal processes. If one assumes that any arbitrary temperature program can be modeled as a series of small time steps,  $t_j$ , where the temperature of each step is  $T(t_j)$ , a continuous cooling/heating is a series of small temperature jumps from the previous step,  $T(t_{j-1})$ , to the current step,  $T(t_j)$ . The fictive temperature of the ith domain at time  $t_i$  is then given by

$$T_{f,i}(t_i) = T(t_i) - [T(t_i) - T_{f,i}(t_{i-1})]\phi_i[t_i, \tau_i(t_i)],$$
 (2)

where each local  $T_{f,i}(t_{j-1})$  relaxes toward the real temperature  $T(t_j)$ , and such a dynamic is governed by the local relaxation function  $\phi_i[t_j,\tau_i(t_j)]$ , which depends on the local relaxation time  $\tau_i(t_j)$ .  $\phi_i[t_j,\tau_i(t_j)]$  generally has a simple exponential form following the assumption of heterogeneous system  $\exp(-\Delta t_j/\tau_{i,j})$ , and  $\Delta t_j = t_j - t_{j-1}$ . The average fictive temperature of the system is then computed according to

$$\langle T_{f,i} \rangle = \sum_{i=1}^{N} W_i T_{f,i}, \tag{3}$$

where  $\langle A \rangle$  is the average value of A. In Refs. 47 and 50, Eq. (3) is the weighted average of local fictive temperature, whose weights are given by the distribution of relaxation times such as the distribution for the KWW equation or Prony series. However, models based on Eq. (2) cannot simulate spatial heterogeneity in the equilibrium states because all  $T_{f,i}$  relax to  $T(t_j)$ , thus the distribution of  $T_f$  vanishes.<sup>52</sup> This contradicts both the experiments and simulations discussed earlier because enthalpy/density fluctuations exist not only in nonequilibrium glassy states but also in the undercooled equilibrium state. These equilibrium distributions are bound to affect the ensuing distribution of glassy  $T_f$  as the system drops out of equilibrium and consequently must directly affect the relaxation dynamic of the glass.

In this work, we therefore develop a model that accounts for both enthalpy fluctuation and temperature-dependent  $\beta_{\text{KWW}}$  in both the nonequilibrium and equilibrium states by introducing the local equilibrium fictive temperature  $T_{f,i}^e$  with weights  $W_i^e$ . A mathematical expression for  $T_{f,i}^e$  is obtained by analyzing the DFDT. Implementation of this model is achieved by extending the TNM model with the help of Cangialosi et al.'s model of temperature-dependent nonexponentiality, with a modification accounting for nonequilibrium states.<sup>53</sup> Our model provides the temperature dependence of  $\beta_{KWW}$ , and the results agree well with experimental measurements. We also simulate volume and enthalpy relaxation far from equilibrium using the seminal study by Scherer<sup>47</sup> and the recent study by Lancelotti et al.48 We show that the present model successfully describes the relaxation dynamics over a broad range of conditions near and far from equilibrium with a single set of parameters, whereas the TNM model fails to do so. The model also provides the temperature dependence of the fluctuation of fictive temperatures,  $\delta T_{\rm f}$ , which is consistent with the DFDT.<sup>54</sup> The evolution of  $\delta T_{\rm f}$  simulated during isothermal annealing for glassy selenium at

different quench rates shows a nonmonotonic evolution consistent with the enthalpy landscape model by Mauro et al. 42,55 However, our simulation predicts that such nonmonotonic evolution only happens when the cooling rate is sufficiently high. In Sec. II, we present the phenomenological model of dynamic heterogeneity in undercooled liquids and glass. In Sec. III A, we apply the present model to four organic systems and two inorganic systems to obtain the model parameters. In Sec. III B, we compare the calculated temperature-dependent nonexponentiality parameters to the experimental ones in undercooled liquid states. In Sec. III C, we study the effect of temperature dependent nonexponentiality far from equilibrium by applying the model to the volume and enthalpy relaxation data in the literature. In Sec. III D, we calculate  $\delta T_f$ with various thermal histories and compare it with experiments. Section III E discusses the nonmonotonic evolution of enthalpy fluctuation by analyzing the results of our model. Finally, Sec. IV concludes this paper with the possibilities and limitations of our model.

### II. HETEROGENEOUS MODEL OF STRUCTURAL RELAXATION IN UNDERCOOLED LIQUID AND GLASS

#### A. Mathematical formulation

In this section, we extend the TNMH model to account for temperature dependent nonexponentiality and enthalpy fluctuations in undercooled liquids and glasses. Existing phenomenological models incorporating heterogeneous relaxation rely on Eq. (2), where all  $T_{\rm f,i}$  relaxes to the single real temperature T in the equilibrium state, which leads to the vanishing of the fluctuation of  $T_{\rm f}$ . However, dynamic heterogeneity is observed in undercooled equilibrium liquids in both experiments and simulations. To overcome this problem, we introduce a new local order parameter called equilibrium fictive temperature,  $T_{\rm f,i}^e$ , which has weights,  $W_i^e$ . The average of  $T_{\rm f,i}^e$  is the real temperature, T, according to

$$\sum_{i=1}^{N} W_{i}^{e} T_{f,i}^{e} = \langle T_{f,i}^{e} \rangle = T, \tag{4}$$

where  $\sum_{i=1}^{N} W_i^e = 1$ . To define  $W_i^e$  in the above-mentioned equation, we rely on Cangialosi et al.'s formulation of dynamic heterogeneity with the assumption that the distribution of local relaxation times (with weights  $X_i$ ) is the same as the distribution of local fictive temperatures (with weights W<sub>i</sub><sup>e</sup>).<sup>53</sup> To model the distribution of relaxation times, Cangialosi et al.'s formulation uses the Vogel-Fulcher-Tamman (VFT) equation, whose parameter Vogel temperature  $T_v$  has a distribution  $g(T_v)$ . Cangialosi et al. assume a linear relation between the distribution of relaxation time  $G(\ln \tau)$  and the distribution of Vogel temperature  $g(T_v)$ . Instead of using the continuous distribution of Vogel temperature  $g(T_v)$  in Cangialosi et al.'s formalism, we use discrete weights  $Y_i$  for each local Vogel temperature  $T_{v,i}$ , where  $g(T_{v,i}) = Y_i$ , and discrete weights  $X_i$  for each local relaxation time  $\tau_i$ , where  $G(\ln \tau_i) = X_i$ . Then, with the above-mentioned assumption,  $W_i^e$  can also be defined in terms of the weights of the Vogel temperature  $Y_i$  as

$$W_i^{\rm e} = \frac{Y_i}{H} \left( \frac{\partial T_{\rm f,i}^{\rm e}}{\partial T_{\rm v,i}} \right)^{-1},\tag{5}$$

where H is the normalization factor so that the above-mentioned equation satisfies  $\sum_{i=1}^{N} W_i^e = 1$ . Therefore, we need to derive an equation for  $T_{t,i}^e$  as a function of  $T_{v,i}$  to determine the second term in Eq. (5). Such an equation can be derived by satisfying the following conditions.

First, an inverse relationship between  $T_{v,i}$  and  $T_{f,i}^e$  is expected. Indeed, it is expected that the relaxation time  $\tau$  increases with decreasing fictive temperature  $T_{f,i}^e$ . However, according to the Vogel–Fulcher–Tamman (VFT) equation, the relaxation time of *i*th domain  $\tau_i$  increases with increasing Vogel temperature  $T_{v,i}$  as

$$\tau_i = \tau_0 \, \exp\left(\frac{DT_{v,i}}{T - T_{v,i}}\right),\tag{6}$$

where D is the strength parameter related to the fragility index.<sup>31</sup> Second, Donth's fluctuation dissipation theorem (DFDT) shows that  $^{26,56}$ 

$$\left| \frac{\partial T_{f,i}^{e}}{\partial T_{v,i}} \right|_{T_{v,i} = \langle T_{v} \rangle} = \frac{T}{\langle T_{v,i} \rangle}. \tag{7}$$

See the supplementary material for the full derivation of Eq. (7). We find that the following equation satisfies both conditions and will, therefore, be used as an expression for  $T_{f,i}^{e}$ , which can be derived to obtain the second term in Eq. (5),

$$T_{\mathbf{f},i}^{\mathbf{e}} = \left\langle T_{\mathbf{f},i}^{\mathbf{e}} \right\rangle \left( 2 - \frac{T_{\mathbf{v},i}}{\left\langle T_{\mathbf{v},i} \right\rangle} \right) = T \left( 2 - \frac{T_{\mathbf{v},i}}{\left\langle T_{\mathbf{v},i} \right\rangle} \right), \tag{8}$$

with the constraint that  $2\langle T_{v,i}\rangle \geq T_{v,i}$  for all  $T_{v,i}$ . Next, we derive an expression for the first term  $Y_i$  for  $W_i^e$  in Eq. (5). In Ref. 53, Cangialosi *et al.* use a Gaussian distribution for the Vogel temperature, which results in the distribution of the log of relaxation time also being Gaussian. However, this is a simplification because the distribution of the log of relaxation time has a long tail in the fast relaxation time region, which is intrinsic to nonexponential relaxation. Typically, such a distribution can be expressed by the probability density distribution of the KWW equation  $G_{KWW}(\ln \tau)$ , which can be numerically calculated as suggested by Lindsey and Patterson, and Patterson, Therefore, in order to use the more appropriate distribution of the weights for the local relaxation time  $X_i$ , we first write the expression for  $Y_i$  in terms of  $X_i$  following Ref. 53 as

$$Y_i = \frac{X_i}{I} \left( \frac{\partial T_{v,i}}{\partial \ln \tau_i} \right)^{-1},\tag{9}$$

where *I* is the normalization factor so that  $\sum_{i=1}^{N} Y_i = 1$ . The first term  $X_i$  can be computed by  $G_{\text{KWW}}(\ln \tau_i)$  as

$$X_i = \frac{G_{\text{KWW}}(\ln \tau_i)}{I},\tag{10}$$

where J is the normalization factor so that  $\sum_{i=1}^{N} X_i = 1$ . Because  $Y_i$  does not depend on temperature, we can compute  $Y_i$  at a given temperature. We define this reference temperature of  $G_{KWW}(\ln \tau_i)$  to be  $T_g$ , where the average relaxation time at  $T_g \langle \tau_i(T_g) \rangle$  is defined

as 100 s. In addition, we denote the reference set of  $X_i$  as  $X_i^{\text{ref}}$ .  $G_{\text{KWW}}(\ln \tau_i)$  can be numerically calculated by 58

$$G_{\text{KWW}}\left[\ln\left(\tau_i/\tau_{\text{KWW}}\right)\right] = \sum_{n=1}^{\infty} \frac{\left(-1\right)^n}{n!} \frac{\left(\tau_i/\tau_{\text{KWW}}\right)^{nf}}{\Gamma(nf)},\tag{11}$$

where  $\Gamma$  is the gamma function and f determines the nonexponentiality of the distribution of local relaxation time, which varies as  $0 < f \le 1$ .  $\tau_{KWW}$  is calculated by  $\tau_{KWW} = \langle \tau_i \rangle / \Gamma \left( \frac{1}{f} + 1 \right)$ , where we use  $\langle \tau_i \rangle$  as the average relaxation time at  $T_g \langle \tau_i (T_g) \rangle$ , which is assumed to be 100 s. The range of  $\tau_i / \tau_{KWW}$  should be appropriately defined to encompass the full spectrum of  $G_{KWW}[\ln (\tau_i / \tau_{KWW})]$ .

Obtaining the second term of Eq. (9) requires an expression for  $T_{v,i}$  as a function of  $\ln \tau_i$ . This is performed by solving Eq. (6) for  $T_{v,i}$  at  $T_{\rm g}$  as

$$T_{v,i}[\ln\left(\tau_i(T_g)\right)] = \frac{T_g}{1 + \frac{D}{\ln\left(\frac{\tau_i(T_g)}{\tau_0}\right)}}.$$
 (12)

By taking the partial derivative of Eq. (12) with respect to  $\ln \tau_i(T_{\rm g})$ , we get the second term of Eq. (9) as

$$\left(\frac{\partial T_{v,i}}{\partial \ln \tau_i(T_g)}\right)^{-1} = \frac{1}{T_g D} \left(\ln \left(\frac{\tau_i(T_g)}{\tau_0}\right) + D\right)^2.$$
 (13)

By inserting Eqs. (10), (11), and (13) into Eq. (9), we get  $Y_i$  as

$$Y_{i} = \frac{1}{I} \frac{1}{T_{g}D} \left( \ln \left( \frac{\tau_{i}(T_{g})}{\tau_{0}} \right) + D \right)^{2} \sum_{n=1}^{\infty} \frac{\left(-1\right)^{n}}{n!} \frac{\left(\tau_{i}(T_{g})/\left\langle \tau_{i}(T_{g})\right\rangle\right)^{nf}}{\Gamma(nf)}. \tag{14}$$

Finally, the full expression for  $W_i^{\rm e}$  can be obtained by taking the partial derivative of Eq. (8) and inserting it with Eq. (14) into Eq. (5) as

$$W_{i}^{e} = \frac{1}{H} \frac{1}{T_{g}D} \left( \ln \left( \frac{\tau_{i}(T_{g})}{\tau_{0}} \right) + D \right)^{2}$$

$$\times \sum_{v=1}^{\infty} \left[ \frac{(-1)^{n}}{n!} \frac{\left(\tau_{i}(T_{g})/\langle \tau_{i}(T_{g})\rangle\right)^{nf}}{\Gamma(nf)} \right] \left( -\frac{\langle T_{v,i}\rangle}{\langle T_{e,i}^{e}\rangle} \right), \quad (15)$$

where  $\langle T_{f,i}^e \rangle = T$  in Eq. (4). Notice that if one calculates the normalization factor H, it will cancel the last term in the parenthesis. This is because they are the macroscopic variables, not the local quantity; hence,  $W_i^e = Y_i$ . This is a consequence of the result of Eq. (8), where the partial derivative of Eq. (8) only leaves the macroscopic variables  $\langle T_{f,i}^e \rangle$  and  $\langle T_{v,i} \rangle$ . We will see that this is not the case when we derive an expression for  $X_i$  in terms of  $Y_i$  in Sec. II B. The second assumption of this model is that the distribution of equilibrium local fictive temperature gets frozen when the system drops out of equilibrium; therefore, we use the equivalency  $W_i^e = W_i$ . Therefore, the distribution of local fictive temperature can also be calculated using Eq. (15) by replacing  $\langle T_{f,i}^e \rangle$  by  $\langle T_{f,i}^e \rangle$ .

Now that we have an expression for  $W_i$ , we can compute  $\langle T_{f,i} \rangle$  using Eq. (3). By following the TNMH and KAHR approaches as in Eq. (2), we assume that any arbitrary thermal change can be modeled

by a series of temperature steps. Furthermore, we assume that local  $T_{f,i}$  relaxes toward local  $T_{f,i}^e$  according to a local relaxation function,  $\phi_i[t_i, \tau_i(t_i)]$ . Therefore, we can rewrite Eq. (2) as

$$T_{f,i}(t_j) = T_{f,i}^{e}(t_j) - \left[T_{f,i}^{e}(t_j) - T_{f,i}(t_{j-1})\right] \phi_i[t_j, \tau_i(t_j)].$$
 (16)

Following Cangialosi *et al.*,<sup>53</sup> we assume that the relaxation of each local domain in a single time step is governed by:

$$\phi_i[t_j, \tau_i(t_j)] = \exp\left(-\left(\frac{\Delta t_j}{\tau_i(t_j)}\right)^{\beta_0}\right),\tag{17}$$

where  $\beta_0$  is called intrinsic nonexponentiality. It is the nonexponentiality of a local domain. This form follows a model developed by Richert and Richert.  $^{60}$   $\beta_0 = 1$  leads to the heterogeneous limit, where the dispersion of the macroscopic relaxation function solely comes from the distribution of relaxation time  $G(\ln \tau_i)$ . In the homogeneous extreme,  $\beta_0$  is inherent to each relaxing unit and, therefore, controls the macroscopic relaxation function.  $^{61}$ 

The local relaxation time  $\tau_i$  in Eq. (17) must be obtained using a model for undercooled liquid and glass. <sup>10,62</sup> In this study, we use the form of the Adam–Gibbs equation modified by Hodge as <sup>63</sup>

$$\tau_i = \tau_0 \exp\left(\frac{DT_{v,i}}{T\left(1 - \frac{T_{v,i}}{\langle T_{f_i} \rangle}\right)}\right). \tag{18}$$

Here,  $\langle T_{f,i} \rangle$  is used instead of  $T_{f,i}$ . This treatment is based on the heterogeneous model of enthalpy relaxation proposed by Richert in Ref. 51.

Finally, we can calculate the global relaxation function,  $\Psi(T_{f_i}(t))$ , between arbitrary time intervals from  $t_0$  to  $t_1$  as

$$\Psi(\langle T_{f,i}(t)\rangle) = \frac{\langle T_{f,i}(t)\rangle - \langle T_{f,i}(t_0)\rangle}{\langle T_{f,i}(t_1)\rangle - \langle T_{f,i}(t_0)\rangle}.$$
 (19)

Equation (19) includes the effect of nonlinearity on temperature and fictive temperature dependent nonexponentiality during relaxation.

In practice, the computation takes place as in the TNMH or the KAHR models. If one considers a simple heating experiment, above  $T_{\rm g}$ , the  $\tau_i$  in Eq. (17) becomes shorter than  $\Delta t_j$ , thus,  $\langle T_{{\rm f},i} \rangle$  relaxes to  $\langle T_{{\rm f},i}^{\rm e} \rangle$  and  $\langle T_{{\rm f},i} \rangle = \langle T_{{\rm f},i}^{\rm e} \rangle = T$ . We find that 0.1 °C is enough as the temperature step of each time step  $\Delta T(t_j)$  to model the DSC curves of a system, where the time step  $\Delta t_j$  in Eq. (17) is chosen depending on the rate of temperature ramp  $\theta(t_j)$  as  $\Delta t_j = \Delta T(t_j)/\theta(t_j)$ . Furthermore, 200 terms are sufficient to simulate both DSC curves and the relaxation during isothermal annealing below  $T_{\rm g}$  for N in Eq. (3). In the current study, we simulate the isothermal annealing below  $T_{\rm g}$  by using the method proposed by Hodge and Berens to reduce the computational cost. We partition the annealing time into 500 subintervals, which are spaced equally in the log timescale.

Furthermore, the difficulty of converging Eq. (11) is discussed by Lindsay and Patterson. Therefore, we use a library containing  $G_{\rm KWW}[\ln{(\tau_i(T_{\rm g})/\tau_{\rm KWW})}]$  and  $\ln{(\tau_i(T_{\rm g})/\tau_{\rm KWW})}$  calculated by Eq. (11) for each f, where f is varied from 0.1 to 0.95 with a step,  $\Delta f = 0.01$ . Therefore, the fitting algorithm takes the  $G_{\rm KWW}[\ln{(\tau_i(T_{\rm g})/\tau_{\rm KWW})}]$  and  $\ln{(\tau_i(T_{\rm g})/\tau_{\rm KWW})}$  of the selected f from the library to minimize the calculation time and to avoid

potential divergence of Eq. (10) during fitting. The relaxation data for the fitting procedure can be structural relaxation data during isothermal annealing, the normalized heat capacity during heating and cooling measured by DSC, or the time-correlation function measured by dielectric spectroscopy.

We emphasize that our formalism is different from the phenomenological heterogeneous models such as the heterogeneous version of TNMH,  $^{47}$  KAHR,  $^{49,51}$  and the phenomenological model using the Prony series.  $^{50}$  In these models,  $W_i$  is temperature independent, and  $T_{\mathrm{f},i}$  relaxes to the real temperature T, as shown in Eq. (2). This causes the vanishing of the fluctuation of  $T_{\mathrm{f}}$  in the equilibrium state, which contradicts the observations from the experiments and the simulations. Instead, in the present model,  $W_i$  in the glass depends on both the real temperature and the average fictive temperature, as in Eq. (15).

Furthermore, the important advantage of our model is that one can easily modify the shape of the distribution by using a different distribution function for  $T_{v,i}$  than Eq. (11). It is even possible to use bimodal distribution for  $T_v$  to model inhomogeneous media.

## B. Calculation of instantaneous global relaxation function and nonexponentiality parameter of KWW equation

To calculate the temperature and fictive temperature dependent nonexponentiality,  $\beta_{\rm KWW}(T,\langle T_{\rm f,i}\rangle)$ , we need to determine a relaxation function derived from our model that can be fitted with the KWW equation in Eq. (1). We define a function  $\chi(t,T,\langle T_{\rm f,i}\rangle)$  to be the instantaneous global relaxation function as

$$\chi(t', T, \langle T_{f,i} \rangle) = \sum_{i=1}^{N} X_i \phi_i [t', \tau(T, \langle T_{f,i} \rangle)], \qquad (20)$$

where  $\phi_i[t', \tau(T, \langle T_{f,i} \rangle)]$  is the local relaxation function of Eq. (17), and t' is the dummy time variable whose range must be appropriately defined to get the full spectrum of  $\chi(t', T, \langle T_{f,i} \rangle)$ .  $\tau_i(T, \langle T_{f,i} \rangle)$  is calculated by Eq. (18), and  $X_i$  can be expressed in terms of  $Y_i$  by rearranging Eq. (9) as

$$X_i = \frac{Y_i}{L} \left( \frac{\partial \ln \tau_i}{\partial T_{v,i}} \right)^{-1}, \tag{21}$$

where  $Y_i$  is in Eq. (14) and the second term can be calculated from Eq. (18). Then, the above-mentioned equation becomes

$$X_{i} = \frac{Y_{i}}{L} \frac{T}{D} \left( 1 - \frac{T_{v,i}}{\langle T_{f,i} \rangle} \right)^{2} = X_{i}^{\text{ref}} \frac{TT_{g}}{\langle T_{f,i} \rangle^{2}} \left( \frac{\langle T_{f,i} \rangle - T_{v,i}}{T_{g} - T_{v,i}} \right)^{2}.$$
 (22)

 $\chi(t,T,\langle T_{f,i}\rangle)$  is different from the global relaxation function  $\Psi$  in Eq. (19) because  $\chi(t,T,\langle T_{f,i}\rangle)$  does not depend on the time evolution of  $\langle T_{f,i}\rangle$ . Equation (20) is the extended version of the time-correlation function in Ref. 53, where  $\chi(t,T,\langle T_{f,i}\rangle)$  is equivalent to the time-correlation function of Ref. 53 in the equilibrium state,  $\langle T_{f,i}\rangle = T$ . We fit  $\chi(t,T,\langle T_{f,i}\rangle)$  by the KWW equation of Eq. (1) to obtain  $\beta_{\text{KWW}}(T,\langle T_{f,i}\rangle)$ . From Eq. (22), we can notice that  $X_i$  is determined by  $Y_i$ , and the term inside the parentheses depending on the value of  $T_{v,i}$ . Therefore, contrary to  $W_i^e, X_i \neq Y_i$ .

The temperature dependent nonexponentiality in equilibrium state,  $\langle T_{f,i} \rangle = \langle T_{f,i}^e \rangle = T$ , can be obtained by substituting  $\langle T_{f,i}^e \rangle$  to T in Eqs. (18) and (22).

### **III. RESULTS AND DISCUSSION**

### A. Obtaining model parameters by fitting calorimetric data

To test the model, we study four organic systems: glycerol, OTP, PVAc, and D-sorbitol, and two inorganic systems: selenium and B2O3. These systems were chosen because (1) the calorimetric data are available for all systems, (2) they cover a wide range of fragility indexes, and (3) the temperature-dependent nonexponentiality ( $\beta_{KWW}$ ) is available for some of these systems in the literature. First, we fit our model to the calorimetric data obtained by DSC. It is preferred to fit multiple data with different thermal histories simultaneously to capture the wide range of thermal history dependence of the glass transition. We fit the calorimetric data available in the literature where the cooling rate was varied as shown in the legend in Fig. 1, and the heating rate used for each system is denoted as  $\theta_h$  in the legend of Fig. 1. For organic systems such as glycerol and PVAc,  $\beta_0$  was estimated from the data of temperaturedependent  $\beta_{KWW}$ , where it is assumed to be the high-temperature limit of  $\beta_{KWW}$ .<sup>53</sup>  $\beta_0$  of selenium, B<sub>2</sub>O<sub>3</sub>, OTP, and D-sorbitol are assumed to be one. The heat capacity around the glass transition measured by DSC can be normalized by fitting the glassy heat capacity,  $C_{p,g}$ , and liquid heat capacity,  $C_{p,l}$ , with a linear equation  $C_p(T) = aT + b$ . Then, the normalized heat capacity,  $\overline{C_p}$ , is calculated by  $\overline{C_p} = (C_p(T) - C_{p,g}(T))/(C_{p,l}(T) - C_{p,g}(T))$ , where  $\overline{C_p}$  is equivalent to  $d\langle T_f \rangle/dT$ . The fitting was performed by the leastsquare method with the optimization code found in the SciPy package in Python.<sup>64</sup>  $\beta_0$  for B<sub>2</sub>O<sub>3</sub>, Se, OTP, and D-sorbitol are fixed at 1 and that for PVAc and glycerol is 0.85 and 0.82, respectively. The results of fitting are shown in Fig. 1. The fitting quality is reasonable for all systems in this study, where the R-squared value for each fit is shown in the legend denoted as  $R^2$ .  $T_g$  is then obtained from the fitting procedure by

$$T_{\rm g} = \langle T_{{\rm v},i} \rangle \left( 1 + \frac{D}{\ln \left( \frac{\tau_i(T_{\rm g})}{\tau_0} \right)} \right),$$
 (23)

where  $\langle \tau_i(T_g) \rangle$  is 100 s. The fragility indices, m, are also obtained from the fitting procedure by

$$m = \frac{D\langle T_{v,i} \rangle T_g}{(T_g - \langle T_{v,i} \rangle)^2 \ln 10}.$$
 (24)

The four fitting parameters  $T_{\rm g}$ , m,  $\log_{10} \tau_0$ , and f for each system are compiled in Table I. The values of  $X_i^{\rm ref}$  and  $\ln \tau_i/\tau_{\rm KWW}$  for each f are listed in the supplementary material. The calculated m for each system is also shown in Fig. 2(a), along with those obtained experimentally. The m calculated from the best-fit parameters is in excellent agreement with the literature value, as most of the m values lie along the diagonal line except for OTP. This deviation for OTP is likely caused by the lack of calorimetric data used in this study, where only one cooling/heating scan was used.

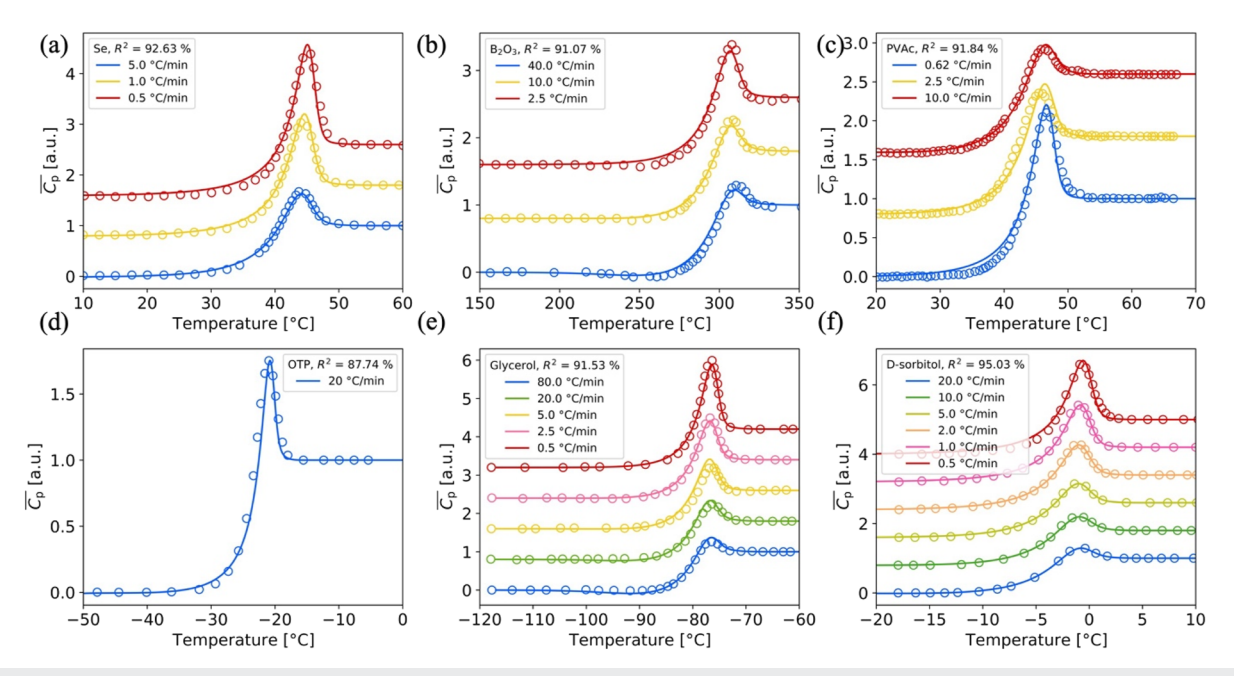


FIG. 1. Best fits of calorimetric data obtained by the least-squared optimization for selenium (a), B<sub>2</sub>O<sub>3</sub> (b), PVAc (c), OTP (d), glycerol (f), and D-sorbitol (g). Open dots represent the measured heat capacity, which was normalized according to the Moynihan method (details in the main text). Data for selenium, B<sub>2</sub>O<sub>3</sub>, PVAc, glycerol, and D-sorbitol are from Refs. 65–70, respectively. The cooling rate for each system is labeled in the inset, while the heating rate and the optimized model parameters for each system are in Table I.

**TABLE I.** The four model parameters obtained from the fitting procedure illustrated in Fig. 1.  $T_g$  is in Kelvin,  $\tau_0$  is in s, and f is the shape parameter for the weights of  $T_{v,i}$  in Eq. (14).

System	$T_{ m g}$	m	$\log_{10}  au_0$	f
Se	308.13	64.14	-23.41	0.59
$B_2O_3$	559.66	36.28	-15.39	0.60
Glycerol	189.73	52.25	-25.40	0.64
OTP	246.15	106.16	-25.48	0.59
PVAc	313.06	92.36	-37.87	0.52
D-sorbitol	265.7	88.76	-35.61	0.57

### B. Temperature-dependent nonexponentiality

To obtain  $\beta_{\rm KWW}$  for arbitrary temperatures, we first calculate the instantaneous global relaxation functions,  $\chi(t',T,\langle T_{\rm f,i}\rangle)$ , by using Eq. (20) at arbitrary temperatures during cooling at 10 °C/min. These functions are then fitted with the KWW equation in Eq. (1) to obtain  $\beta_{\rm KWW}$  at each temperature. The distribution of relaxation times  $G(\log_{10}\tau_i)$  is calculated from their weights  $X_i$  by normalizing them by  $\sum_{i=1}^{N-1} X_i (\log_{10}\tau_{i+1} - \log_{10}\tau_i)$ , thus the area under  $G(\log_{10}\tau_i)$  becomes one.  $G(\log_{10}\tau_i)$  and the corresponding calculated  $\chi(t',T,\langle T_{f,i}\rangle)$  for  $B_2O_3$  are shown in Fig. 3. The dashed lines in Fig. 3(a) are the distribution of equilibrium relaxation time,  $G(\log_{10}\tau_i^e)$ , and solid lines are those of nonequilibrium relaxation time,  $G(\log_{10}\tau_i^e)$ .  $G(\log_{10}\tau_i^e)$  is calculated from  $X_i$  by substituting  $\langle T_{f,i}\rangle$  by T in Eqs. (18) and (22). The most important feature in

Fig. 3(a) is that  $G(\log_{10}\tau_i)$  and  $G(\log_{10}\tau_i^e)$  are narrower for higher temperatures. This is the well-known temperature dependence of the distribution of relaxation time in a system that exhibits temperature dependent nonexponentiality. At high temperatures above  $T_g$  (where  $T_g$  of  $B_2O_3$  is around 270 °C), the  $G(\log_{10}\tau_i^e)$  (dashed lines) and  $G(\log_{10}\tau_i)$  (solid lines) overlap. However,  $G(\log_{10}\tau_i)$  starts to diverge from  $G(\log_{10}\tau_i^e)$  below  $T_g$ , where the solid lines at T < 270 °C remain in the short relaxation time range while the dashed lines at the same temperatures have a much longer relaxation time. This means that  $G(\log_{10}\tau_i)$  was frozen during the glass transition. Figure 3(b) shows  $\chi(t', T, \langle T_{f,i} \rangle)$  from Eq. (20) as solid lines and the fitted KWW equation of Eq. (1) as dashed lines. They overlap almost perfectly, indicating that  $\chi(t', T, \langle T_{f,i} \rangle)$  does not have a nonlinearity effect ( $\langle T_{f,i} \rangle$  is constant over all t').

The obtained  $\beta_{\rm KWW}$  at  $T_{\rm g}$  for both equilibrium (solid circles) and nonequilibrium (open circles) are compared with the experimentally measured  $\beta_{\rm KWW}$  in Fig. 2(b), which is taken from Refs. 31 and 76–80. The calculated  $\beta_{\rm KWW}(T_{\rm g})$  from the optimized parameters agrees well with the measured  $\beta_{\rm KWW}(T_{\rm g})$  for most of the system except D-sorbitol (red circle). While it is unclear why such a large overestimation of  $\beta_{\rm KWW}(T_{\rm g})$  occurs for D-sorbitol, the larger value of  $\beta_{\rm KWW}(T_{\rm g})$  obtained by fitting the TNMH model to the DSC curves of D-sorbitol was already observed in Ref. 70. In addition, we can see that  $\beta_{\rm KWW}$  for both equilibrium and nonequilibrium are not equal even at  $T_{\rm g}$ . This is caused by the distribution of nonequilibrium relaxation time, which already deviates from that of equilibrium relaxation time during cooling. Overall, the obtained  $\beta_{\rm KWW}$  for all systems is in good agreement with the experimental

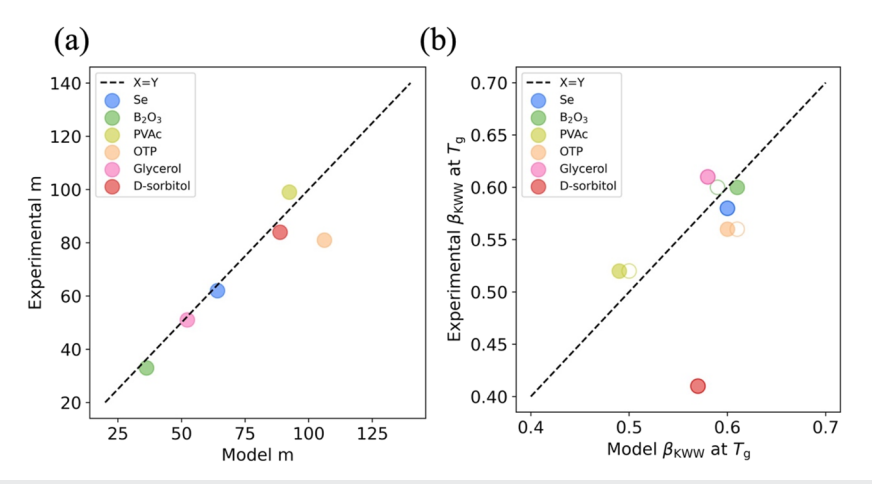
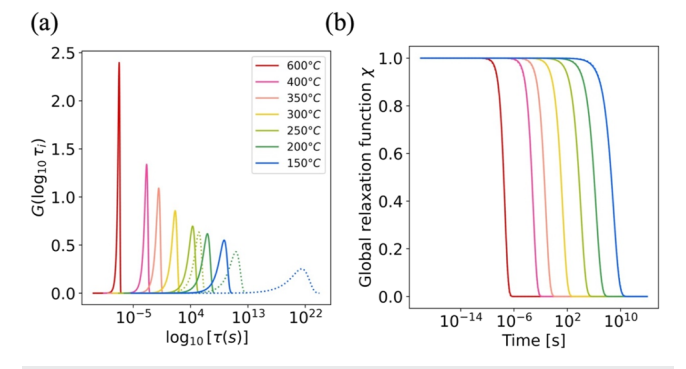


FIG. 2. (a) Comparison between calculated fragility indices, m, using Eq. (24) and experimental fragilities. The measured fragilities of selenium, B $_2$ O $_3$ , PVAc, OTP, glycerol, and D-sorbitol are from Refs. 67 and 71 75, respectively. (b) Comparison between the calculated nonexponentiality parameter of both equilibrium (solid circles) and nonequilibrium (open circles) states at  $T_g$  and the experimental  $\beta_{KWW}$  at  $T_g$ . The experimental  $\beta_{KWW}$  ( $T_g$ ) of OTP, PVAc, glycerol, and D-sorbitol are from Refs. 76–79. The experimental  $\beta_{KWW}$  ( $T_g$ ) of selenium and B $_2$ O $_3$  are from Refs. 31 and 80. The black dashed line is when the obtained value and the experimental value are equal.

values at  $T_g$ . The obtained  $\beta_{KWW}$  at various temperatures for  $B_2O_3$ , glycerol, OTP, and PVAc are compared with experimental data in Figs. 4(a)-4(d). The red circles in the figures are the calculated  $\beta_{KWW}$  obtained using the weights and the local relaxation time in the equilibrium state, whereas the orange circles are the ones obtained using  $\tau_i$  and  $X_i$  in the nonequilibrium state. Dashed lines are guides to the eye. Unfortunately, experimental data on temperature-dependent  $\beta_{KWW}$  for selenium and D-sorbitol were not available in the literature. All the calculated results show good agreement with the literature. As expected from the deviation of  $G(\log_{10}\tau_i)$  from  $G(\log_{10}\tau_i^e)$  shown in Fig. 3,  $\beta_{KWW}$  obtained from  $G(\log_{10}\tau_i)$  starts to diverge from that obtained from  $G(\log_{10}\tau_i^e)$ . This was also predicted by RFOT theory. It is important to note that the



**FIG. 3.** (a) The distribution of relaxation time of  $B_2O_3$  for equilibrium and nonequilibrium state calculated by Eqs. (18) and (22) for various temperatures, where  $\langle T_{f,i} \rangle = T$  for an equilibrium state. Solid lines are the distribution of nonequilibrium relaxation time, and dotted lines are those of the equilibrium state. (b) The instantaneous global relaxation function calculated by Eq. (20) is represented in solid lines, and the fitted KWW function in Eq. (1) is represented in dotted lines. Both lines perfectly overlap.

experimentally measured  $\beta_{\mathrm{KWW}}$  varies between different experimental methods.<sup>82</sup> This is because of the difference in the timescale of particular experiments.83 The data shown in Fig. 4(c) for OTP were taken from the HCS measurements by Dixon and Nagel. The excellent agreement for OTP may be because HCS measures the frequency dependence of enthalpic relaxation processes in the glass transition range. Richert measured the dielectric response of OTP for a wide range of temperatures and frequencies, and the system showed temperature independent nonexponentiality.84 The author mentioned that the difference between Dixon and Nagel's results and the dielectric experiment's results is caused by a small addition of impurity in the sample used in the HCS measurements to avoid crystallization.<sup>73</sup> The excellent agreement between our model's prediction and Dixon and Nagel's results may suggest a potential difference in how the heterogeneity of this system contributes to the enthalpic relaxation and dielectric relaxation processes. For PVAc, while the dielectric measurements of Sasabe and Moynihan<sup>67</sup> above 50 °C show a temperature dependence of nonexponentiality [see Fig. 4(d)], dielectric and mechanical studies by Richert et al. and Zhao et al. find that the nonexponentiality is temperature invariant below 50 °C. 77,85 Further, Zhao et al. find that the temperature dependence of relaxation time in equilibrium states becomes Arrhenius below Tg.77 While it is not clear how this transition of the temperature dependence of relaxation time from non-Arrhenius to Arrhenius affects the temperature dependence of nonexponentiality in PVAc, the current model does not account for such a transition. Therefore, the current model also does not account for the temperature independent nonexponentiality below 50 °C. Nevertheless, our model predicts  $\beta_{\rm KWW}$  by fitting the calorimetric data, which involves the enthalpic relaxation process.

### C. Effect of temperature dependent nonexponentiality near and far from equilibrium

The TNMH and KAHR models have been successful at modeling glass dynamics near equilibrium. 89 However, it has long been

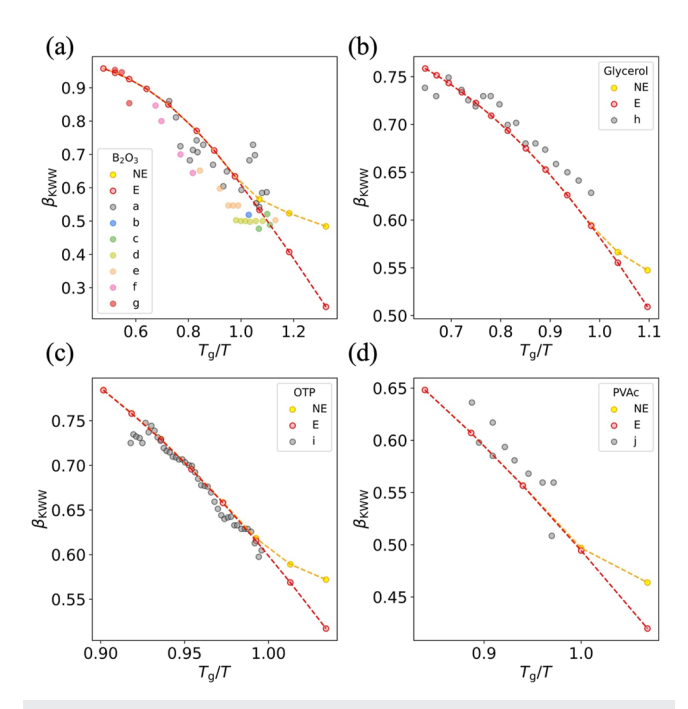


**FIG. 4.** Temperature-dependent  $\beta_{\text{KWW}}$  calculated for  $B_2O_3$  (a), glycerol (b), OTP (c), and PVAc (d) by fitting Eqs. (1)–(20) at various temperatures compared with experimental data (a to j). The red and orange circles represent the values obtained from the distribution of equilibrium relaxation time (E) and nonequilibrium relaxation time (NE), respectively. a is taken from Ref. 86, b to g are from Ref. 87, h is from Ref. 88, i is from Ref. 73, and j is from Ref. 67. Dashed lines are guides to the eye.

known that the TNMH and KAHR models fail to accurately predict structural relaxation after temperature jumps far from equilibrium or after fast quenching from high temperatures. In his seminal paper on volume relaxation far from equilibrium, Scherer already recognized that the relaxation of samples annealed far below  $T_{\rm g}$ could not be fitted with the same set of parameters as samples annealed close to  $T_g$ , using either the TNM equation or the Adam-Gibbs equation for the temperature/fictive temperature dependent relaxation time. 47 Moreover, even when using a separate set of parameters for the samples annealed far from equilibrium (258 °C below their initial fictive temperature), the TNMH model failed to properly fit the sample rapidly quenched from high temperature. This study performed on silicate glass (namely SSG in the following text) required the use of different  $\beta$  values for different conditions. More recently, a study by Lancelotti et al. 48 on lithium disilicate glass (namely LS2 in the following text) showed that both volume and enthalpy relaxation after large and small temperature jumps from equilibrium could not be described with a single set of parameters using the TNMH model. Again, different  $\beta$  values were required for samples annealed far and close to  $T_{\rm g}$ . Both studies, therefore, suggest that thermorheological simplicity is not satisfied for these glass formers.

In the following, we first show the modeling of glass dynamics near equilibrium using Kovacs' seminal volume relaxation data on PVAc.<sup>90</sup> The purpose of this fit is to show that the current

model accounting for temperature dependent nonexponentiality is effective at modeling systems in the temperature ranges where thermorheological simplicity is usually assumed. Second, we model glass relaxation far from equilibrium, where the TNMH model was shown to fail. We show that accounting for temperature dependent nonexponentiality in the present model permits us to simultaneously fit all relaxation data with good accuracy using a single set of four parameters. We emphasize that this is the same number of parameters as the TNMH model. To model all datasets, we fix  $\beta_0$  to 0.85 for PVAc and 1 for the SSG and the LS2, assuming that both silicate glasses are purely heterogeneous.

Kovacs' seminal work on volume relaxation of PVAc shows the complex relaxation dynamics in glassy systems such as the memory effect and the asymmetry of the approach to equilibrium. The data in Fig. 15 of Ref. 90 present the fractional volume relaxation function M(t) measured during isothermal annealing after a temperature down-jump from  $T_0$  at 40 °C to various temperature  $T_a$ . The data from Fig. 17 in Ref. 90 include M(t) measured during isothermal annealing after a temperature up-jump from various temperature  $T_0$  to the annealing temperature  $T_a$  at 40 °C. In Kovacs' work, the volume changes during isothermal annealing V(t) after a jump are normalized by their equilibrium value  $V_\infty$  as

$$M(t) = \frac{|V(t) - V_{\infty}|}{V_{\infty}} = \Delta \alpha (\langle T_{f,i}(t) \rangle - T_{a}), \tag{25}$$

where M(t) is called the fractional deviation. The right-hand side is the expression of M(t) in terms of the macroscopic fictive temperature, where  $\Delta\alpha$  is the difference of the thermal expansion coefficients between liquid  $\alpha_{\rm l}$  and glass  $\alpha_{\rm g}$ .  $\alpha_{\rm l}$  and  $\alpha_{\rm g}$  are assumed to be temperature independent, and they are  $7.175 \times 10^{-4}/{\rm K}$  and  $2.842 \times 10^{-4}/{\rm K}$ , respectively. Alternatively, one can calculate M(t) from the relaxation function in Eq. (19),  $\Psi(t)$  as

$$M(t) = M_{\rm ini} \Psi(t) = M_{\rm ini} \frac{\langle T_{\rm f,i}(t) \rangle - T_{\rm a}}{\langle T_{\rm f,i}(t_{\rm ini}) \rangle - T_{\rm a}}, \tag{26}$$

where  $M_{\rm ini}$  is the initial value of the fractional deviation measured at  $t_{\text{ini}}$ . The term  $t_{\text{ini}}$  is the initial time of the volume measurement, which varies between experimental setups.  $t_{\text{ini}}$  for the Kovacs' set-up is 36 s.<sup>90</sup> We fit the data with the present model, the TNMH model modified by Hodge,<sup>63</sup> with either the Adam-Gibbs (AG) equation or the TNM equation for the relaxation time (the details of the TNMH model are given in Ref. 92, where the model with the AG equation is denoted as the AGS model in the reference). The intrinsic nonexponentiality  $\beta_0$  is fixed at 0.85 as it was performed for the DSC curve fitting for the PVAc. Kovacs' data were taken after thermal equilibration following the temperature jump that took about 36 s.90 Svoboda et al. pointed out that there is a significant information loss during this thermal equilibration before the annealing in the mercury dilatometer. 92 Therefore, we approximate this equilibration period by considering the ramping at the rate estimated by  $(T_a - T_0)/36$  s. The initial value of the fractional deviation during annealing  $M_{\rm ini}$  is calculated using Eq. (25) for different  $T_0$ , and these are compared with the initial data point of Kovacs' data in Fig. s2 in the supplementary material. They show good agreement with the measured initial data point of M for both the present model

and the TNMH models. Finally, M(t) is calculated with Eq. (26), using the simulated  $M_{\rm ini}$  value.

The best fits for PVAc are shown in Fig. 5, where the fits from the current model are in (a), those from the TNMH model with the

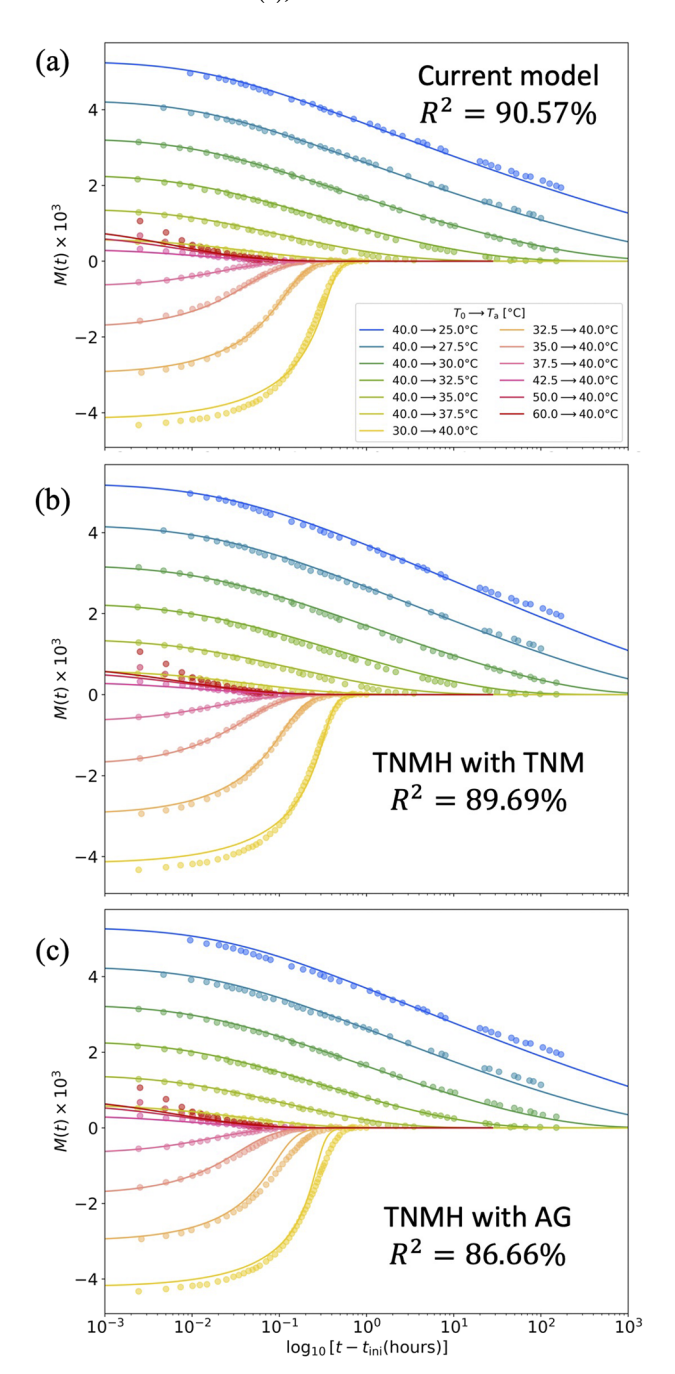


**FIG. 5.** Best fit to Kovacs' volume measurements during annealing from Figs. 15 and 17 of Ref. 90 using the current model in (a), the TNMH model with the TNM equation in (b), and the TNMH model with the AG equation in (c). The initial temperature  $T_0$ , the annealing temperature  $T_a$ , and the total  $R^2$  values are shown in the legend.

**TABLE II.** The four model parameters  $T_g$ , m,  $\log_{10} \tau_0$ , and f obtained from fitting data from Kovacs for the volume relaxation of PVAc Scherer for SSG and Lancelotti *et al.* for LS2.  $\tau_0$  is in s, and f is the shape parameter for the weights of  $T_{v,i}$   $Y_i$  in Eq. (14). The units of each value are the same as those in Table I.

System	$T_{ m g}$	m	$\log_{10}  au_0$	f
PVAc (volume)	311.42	105.93	-22.24	0.48
SSG	827.68	33.56	-12.60	0.67
$LS_2$	737.23	39.01	-21.37	0.88

TNM equation are in (b), and those from the TNMH model with the AG equation are in (c). The optimized parameters, along with the calculated m and  $T_{\rm g}$  for the current model, are compiled in Table II. The values of  $T_g$ , m, and f are fairly similar to the ones obtained by fitting the DSC curves. Although  $\log_{10} \tau_0$  is several orders of magnitude larger than the one from the DSC curve fitting, the difference in  $\log_{10} \tau_0$  between different response functions such as volume and enthalpy is common. 65,67,92,93 The poorer fitting qualities of the data measured after the temperature down-jump from 50 to 60 °C most likely come from the significant information loss during equilibration time, as pointed out by Svoboda et al.,92 as can be seen in the calculated  $M_{\rm ini}$  in Fig. s2 in the supplementary material. The total R-squared values are calculated and shown in the legend, and the plot of the experimental M(t) vs the predicted M(t) for each model is shown in Fig. s3 in the supplementary material. The current model performs the best among the three models tested in this study. Overall, these results and the results of fitting the DSC curves in Sec. III B show that the current model performs well in the temperature range where the standard TNMH model is most extensively

Scherer studied three samples with different thermal histories, each annealed at three different temperatures (500, 450, and 350 °C). "Sample 1" was quenched in a salt bath at 320 °C from 700 °C and had the highest initial fictive temperature  $\langle T_{f,i}(0) \rangle$  of 608.3 °C. "Sample 2" was cooled in air after annealing at 570 °C for 10 mins and had an initial fictive temperature,  $T_{f,i}(0) = 563.1$  °C. "Sample 3" was cooled in air after annealing at 540 °C for 3 h and had the lowest initial fictive temperature,  $T_{f,i}(0) = 539.8$  °C. The cooling rate of the initial quench  $(\theta_{c,1})$  and that during cooling in air  $(\theta_{c,2})$  were not clearly defined in the study; hence, they were presently calculated to yield the corresponding initial fictive temperature before annealing. We find that  $\theta_{c,1} = 57.57$  °C/s and  $\theta_{c,2} = 4.03$  °C/s provide the best results. All datasets were then fitted simultaneously using our model. Table II shows the set of model parameters that gives the best fit to all the volume relaxation data for SSG.  $T_{\rm g}$  is slightly higher than the temperature when the viscosity is  $10^{12}$  Pa s (816 K), and m is also slightly higher than that obtained from the viscosity m = 40.94Fitting results are presented in Fig. 6 and compared with those of the TNMH model. The circles are the data taken from Ref. 47. We reproduce the simulations performed by Scherer with the TNMH model, which includes the continuous cooling effect in dashed lines. Scherer used a single set of parameters obtained by fitting the density changes during annealing at 500 and 450 °C. The R-squared value for each fit is shown in the legend. The results from the present model are in excellent agreement for the entire thermal history considered. However, the TNMH model fails dramatically for the

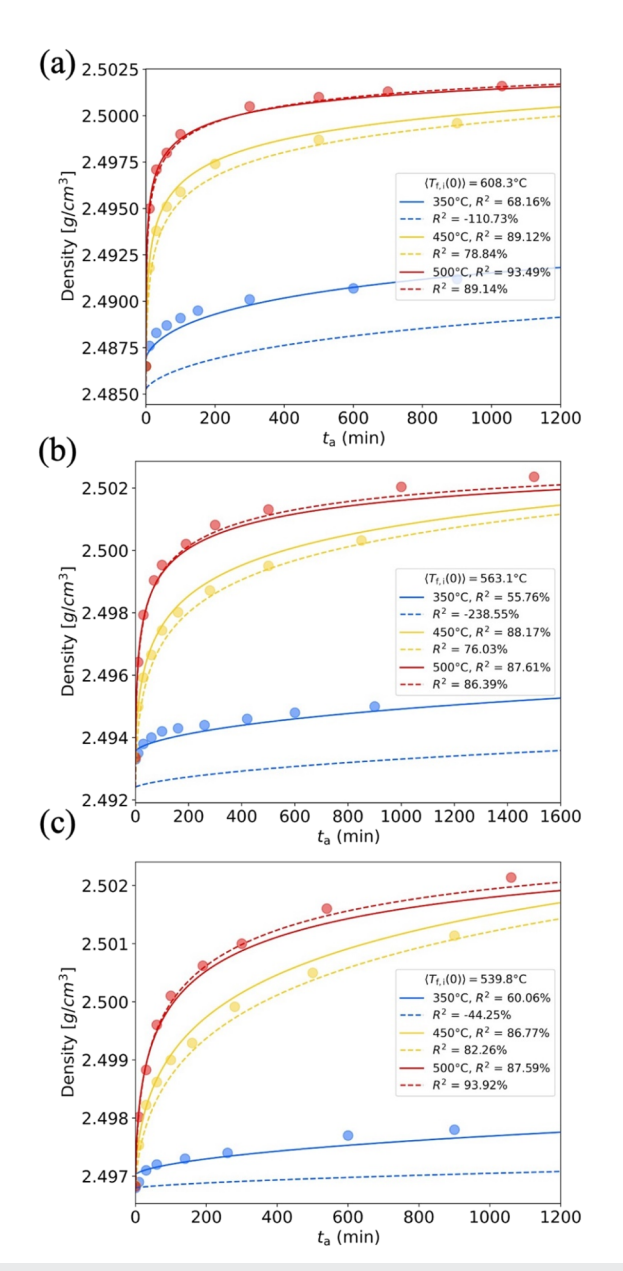


**FIG. 6.** The calculated density changes during annealing from the best fit for sample 1 (a), sample 2 (b), and sample 3 (c). The model parameters are shown in the Table II. The color corresponds to the annealing temperature shown in the legend.  $T_{\rm f}(0)$  in the legend is the initial fictive temperature before annealing. The dashed lines are the results from the TNMH model with the Adam–Gibbs equation in Ref. 47, and the circles are the measured density taken from Ref. 47.

lowest annealing temperature,  $T_a = 350\,^{\circ}\text{C}$ . Considering that the number of fitting parameters in our model is the same as the TNMH model, we conclude that this improvement is the result of accounting for the temperature dependent nonexponentiality in the present model

Scherer also pointed out that even when using a distinct  $\beta$  value for samples annealed at 350 °C, the rate of relaxation of sample 1

was much faster than other samples. To investigate the cause of this fast relaxation, we plotted the temperature dependent  $\beta_{\rm KWW}$  for all samples at various  $T_{\rm a}$  in Fig. 7. The method of obtaining  $\beta_{\rm KWW}$  at an arbitrary temperature and fictive temperature is explained in detail in Sec. III B. It is found that the initial values of  $\beta_{\rm KWW}$  for each sample differ significantly even when they share the same initial fictive temperature,  $\langle T_{f,i}(0) \rangle$ . This is because the weights of relaxation time  $X_i$  not only depend on the average fictive temperature

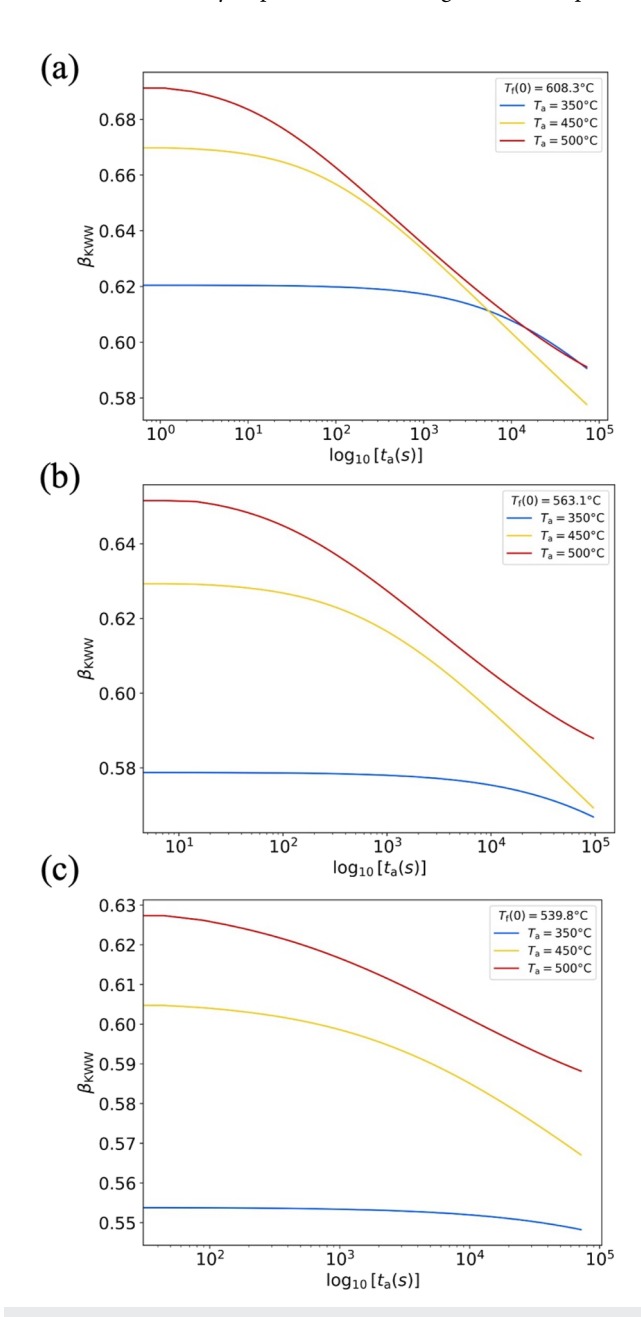


**FIG. 7.** The calculated temperature dependent nonexponentiality obtained from the present model during annealing for sample 1 (a), sample 2 (b), and sample 3 (c). See the text for specific sample conditions.

 $\langle T_{f,i} \rangle$ , but also the actual temperature T [see Eq. (22)]. The higher  $\beta_{\rm KWW}$  for the higher  $T_a$  promotes faster relaxation in addition to the nonlinear effect of the local relaxation time in the sample with the same  $\langle T_{f,i}(0) \rangle$ . The unusually fast relaxation dynamics for sample 1 at 350 °C mentioned earlier can then be explained by the much higher  $\beta_{\rm KWW}$  for sample 1 compared to the other two at 350 °C, where the difference of  $\beta_{\rm KWW}$  between sample 1 and sample 2–3 in the initial stage of relaxation is >0.04. This is due to the high  $\langle T_{f,i}(0) \rangle$  before annealing. This observation supports the conclusion that temperature dependent nonexponentiality is necessary to model relaxation far from equilibrium.

The third set of relaxation data under consideration are the enthalpy and volume relaxation of lithium disilicate glass LS<sub>2</sub> reported by Lancelotti et al.48 after temperature up- and downjump. These relaxation data were analyzed using the TNMH model with the TNM equation for the relaxation time. It was found that the TNMH model requires a different set of model parameters for relaxation after small and large temperature jumps, highlighting that temperature dependent nonexponentiality may be needed. We, therefore, test our model using the enthalpy relaxation data during annealing (1) after the temperature up-jump from 414 to 444 °C, (2) after the temperature up-jump from 414 to 454 °C, and (3) after the temperature down-jump from 454 to 444 °C. We fix  $\beta_0$  to 1 during the fitting; therefore, the number of model parameters is identical to that of the TNMH model. We assumed an infinite cooling rate in this case. The fractional deviation M(t) is calculated from  $\langle T_{f,i}(t) \rangle$  during annealing by Eq. (26), where  $M_{\rm ini}$  is calculated for each data by the equation shown in Ref. 48 and  $\langle T_{f,i}(t_{\text{ini}}) \rangle = T_0$ . The

best-fit parameters are shown in Table II for LS2. The  $T_{\rm g}$  is slightly higher than that obtained by DSC at  $10^{\circ}$ C/min ( $T_{g,DSC} = 727$  K), and m is slightly lower than that calculated from the parameter of the TNMH model in Ref. 48 (m = 47). The results from the best fit are shown in Fig. 8(a), along with the results of Ref. 48. Lancelotti et al. fitted the TNMH model to the data of the small up-jump and the down-jump [see Fig. 7(b)], yielding TNM parameters  $\beta = 0.9$ and x = 0.66. They separately fitted the data of the large up-jump and the down-jump [see Fig. 8(c)], yielding a different set of TNM parameters  $\beta = 0.84$  and x = 0.61. Figure 8(b) shows excellent agreement with the data after the small up-jump and the down-jump, but poor agreement with the data after the large up-jump. Similarly, Fig. 8(c) shows excellent agreement with the data after the large up-jump and the down-jump, but poor agreement with the data after the small up-jump. In contrast, the present model shows excellent agreement across the whole thermal history considered. This again indicates that accounting for temperature dependent nonexponentiality is necessary to describe relaxation over a broad range of departures from equilibrium. Figure 9 shows the temperature dependent  $\beta_{\rm KWW}$  during annealing after each temperature jump. As previously observed,  $\beta_{\rm KWW}$  values are different for different  $T_{\rm a}$  (blue and yellow lines), even when the initial fictive temperature  $T_0$  is the same. This is because the weights of relaxation time not only depend on  $\langle T_{f,i} \rangle$  but also the actual temperature. Similarly, higher  $\beta_{\rm KWW}$  leads to faster relaxation during annealing after the larger temperature jump than the smaller jump,<sup>48</sup> as previously observed. The temperature dependent  $\beta_{\rm KWW}$  also shows an "asymmetry of approach" for samples undergoing a down- and an up-jump.

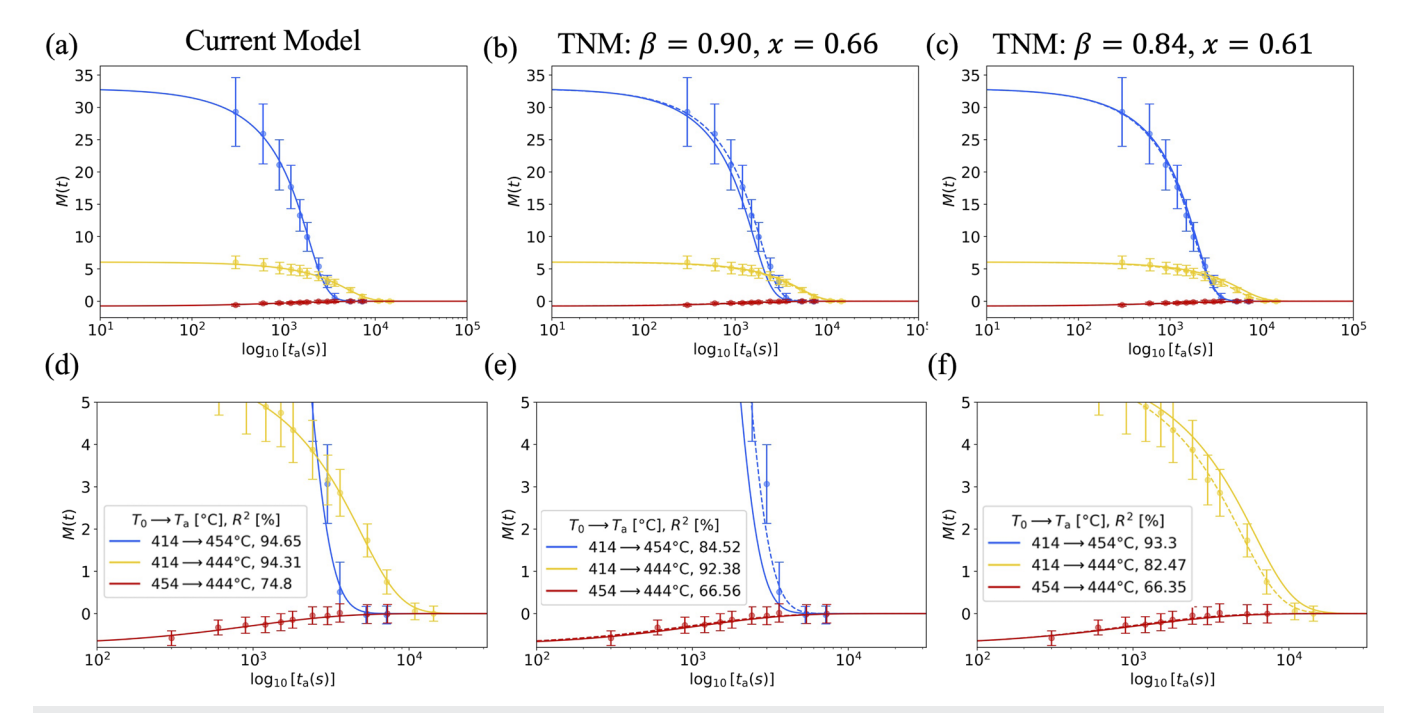
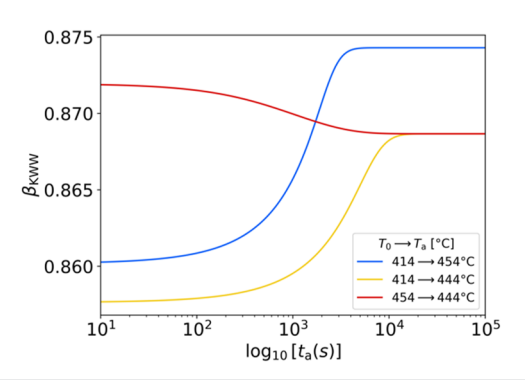


FIG. 8. Fit of enthalpy relaxation data from Ref. 48 using (a) the current model, (b) the TNMH model with best-fit parameters for the small temperature up-jump, and (c) the TNMH model with best-fit parameters for the large temperature up-jump. The dashed lines in (b) and (c) are the results of the present model. The bottom curves are close-up of the upper curves. The current model successfully fits all curves with a single set of parameters.



**FIG. 9.** The temperature dependent  $\beta_{\rm KWW}$  during annealing calculated for different thermal histories.

Overall, the set of results in Figs. 6 and 8 show that the present model can capture full relaxation dynamics during annealing both near and far from equilibrium with a single set of four model parameters (same as the TNMH model). The significant improvement in the fitting suggests that these silicate systems exhibit temperature dependent nonexponentiality, which notably affects relaxation far from equilibrium.

### D. Fictive temperature fluctuation and temperature fluctuation in Donth's fluctuation dissipation theorem

One of the main advantages of the present model is that it can simulate the nonequilibrium dynamics of  $T_{\rm f,i}$  and their weights,  $W_i$ , for arbitrary thermal histories. To quantify the fluctuation of  $T_{\rm f}$ , we calculate the standard deviation of  $T_{\rm f}$  by

$$\delta T_{\rm f} = \sqrt{\sum_{i=1}^{N} W_i (T_{{\rm f},i} - \langle T_{{\rm f},i} \rangle)^2}.$$
 (27)

The connection between the standard deviation and the fluctuation is only rigorous when the distribution has a Gaussian distribution. The fictive temperature in the current model has a non-Gaussian distribution. However, for convenience of the computational process,  $\delta T_f$  is used to quantify the fluctuation of fictive temperature for the purpose of estimating the temperature dependence of the dispersion of the distribution of fictive temperatures. The  $\delta T_{\rm f}$  values calculated using Eq. (27) for B<sub>2</sub>O<sub>3</sub> are shown in Fig. 10(a). The black dashed line is the fluctuation of  $T_f^e$ ,  $\delta T_f^e$ , which can be numerically calculated by substituting  $T_{f,i}$  and  $\langle T_{f,i} \rangle$  to  $T_{f,i}^{e}$ and  $\langle T_{f,i}^e \rangle$  in Eq. (27), or it can be calculated analytically using Eq. (s4) in the supplementary material. Blue and orange lines are the  $\delta T_f$  during cooling and heating at 10 °C/min, respectively. From the figures, we can make the following observations: (1)  $\delta T_f^e$  is narrower for lower temperature, and (2)  $\delta T_f$  narrows rapidly and more significantly during cooling when the system approaches its glass transition. A similar narrowing behavior was observed in the distribution of the molar volume of selenium simulated with the enthalpy landscape model of Mauro and Loucks.<sup>41</sup> It was also inferred by Moynihan and Schroeder from light scattering experiments.<sup>39</sup> During heating, (1)  $\delta T_f$  increases during the glass transition, (2) it becomes broader than the one of  $\delta T_{\rm f}^{\rm e}$  at the same temperature (overshooting of  $\delta T_f$ ), and (3) it decreases to  $\delta T_{\rm f}^{\rm e}$  after the system reaches its equilibrium state. This overshooting of  $\delta T_{\rm f}$  was inferred from the light scattering experiment on B<sub>2</sub>O<sub>3</sub> by Bokov,<sup>38</sup> interpreted by Moynihan and Schroeder.<sup>39</sup> It is caused by heterogeneous enthalpic recovery, where the fast relaxation domains rise to the corresponding equilibrium state faster than the slower domains, which causes the broadening of the distribution. It is interesting to note that the  $\delta T_{\rm f}$  broadens upon cooling below  $T_{\rm g}$ . This is because the domains with lower  $T_{\rm v,i}$  (high  $T_{\rm f,i}^{\rm e}$ ) have relaxation times that have a weaker temperature dependence [see Eq. (18)] than those with higher  $T_{\rm v,i}$ . This causes the domains with high  $T_{\rm v,i}$  to freeze at a higher  $T_{\rm f,i}$  than those with low  $T_{\rm v,i}$ . Therefore, even when the domains with high  $T_{\rm v,i}$  are frozen around  $T_{\rm g}$ , those with lower  $T_{\rm v,i}$  still relax to the lower  $T_{\rm f,i}$ . This causes a broadening of the distribution of  $T_{\rm f,i}$  below  $T_{\rm g}$ .

To compare the  $\delta T_{\rm f}$  to the  $\delta T$  of the DFDT, we simulate TMDSC by using our model. The implementation of TMDSC in the phenomenological model is described in the literature. <sup>95,96</sup> We used the sinusoidal temperature oscillation during heating with the TMDSC parameters shown in Table III. We used the signal processing of TMDSC developed by Wunderlich and Boller. <sup>97</sup>  $\delta T$  was obtained by fitting the Gaussian function to the calculated imaginary part of the complex heat capacity  $C_p$  following the treatment proposed by Hensel and Schick, <sup>98</sup> and an example is shown in Fig. 10(b). Figures 10(c) and 10(d) compare the calculated  $\delta T$  and  $\delta T_{\rm f}^{\rm e}$  with the experimental  $\delta T$  measured by either TMDSC or DSC. <sup>27</sup> The method of estimating  $\delta T$  from conventional DSC is shown in Ref. 99. Overall,  $\delta T_{\rm f}^{\rm e}$  follows the values of the measured  $\delta T$  and the  $\delta T$  obtained by fitting the Gaussian function to the simulated  $C_p$  ". This result suggests that  $\delta T_{\rm f}^{\rm e}$  is consistent with  $\delta T$  in the DFDT.

### E. Enthalpy fluctuation during isothermal annealing below $T_{\rm g}$

Several experimental studies and simulations based on the enthalpy landscape model show a nonmonotonic evolution of density or enthalpy fluctuations during isothermal annealing below  $T_{\rm g}$ . The enthalpy landscape models show that the width of the density distribution first narrows and subsequently increases after it reaches a minimum during isothermal annealing. It was confirmed by experiments conducted using the SAXS and TMDSC. 42,55 This nonmonotonic evolution of the density fluctuation is caused by the spatial heterogeneity of a system. This evolution can be explained in the following two steps: (1) when the temperature was dropped to an annealing temperature,  $T_a$ , the domains with a short relaxation time relax faster than those with a long relaxation time; and (2) after some time, the domains with a long relaxation time relax while those with a short relaxation time are already relaxed in their equilibrium state. The first step causes the narrowing of the spatial distribution of density/enthalpy, and the second step causes the broadening of the distribution. While Mauro investigated its dependence on the initial temperature  $(T_0)$  before quenching and fragility using the enthalpy landscape model, 100 the cooling rate dependence has not been explored.

To investigate the cooling rate dependence on enthalpy fluctuation, we simulated isothermal annealing using our model for selenium. The system was cooled from just above  $T_{\rm g}$  at 40 °C to  $T_{\rm a}$  at 25 °C at various cooling rates from 0.2 to 10<sup>6</sup> °C/s, and then

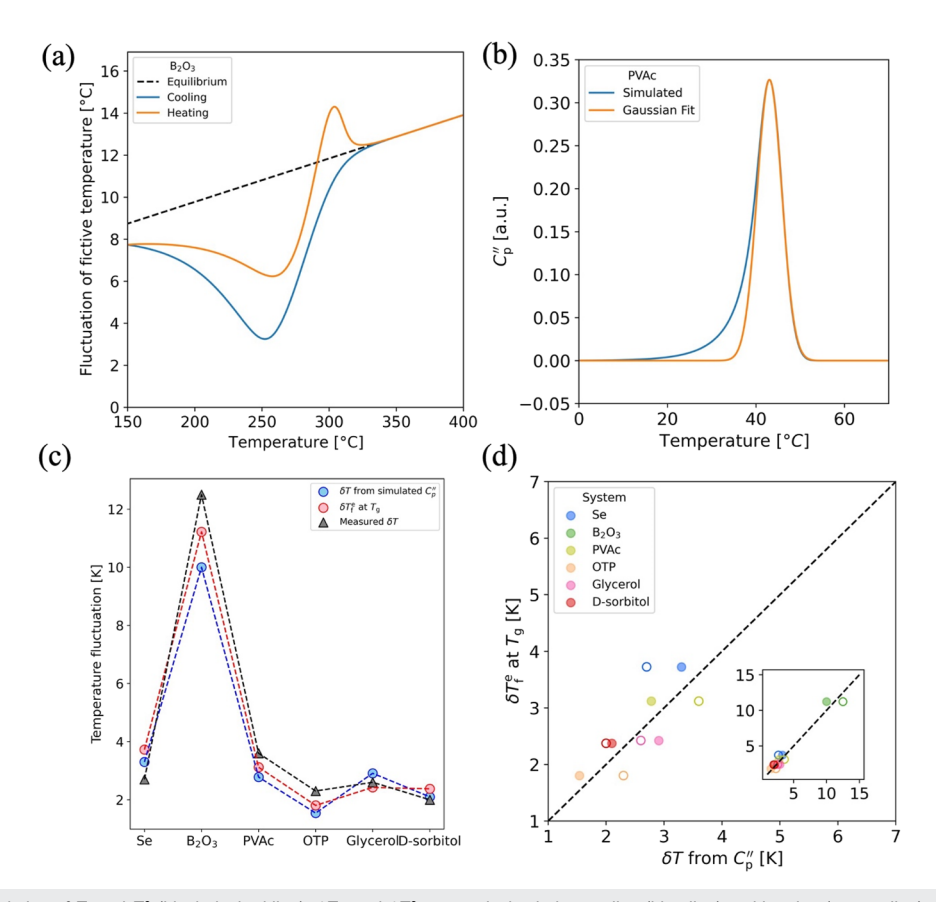


**FIG. 10.** (a) Standard deviation of  $T_f$  (black dashed line),  $\delta T_f$ , and  $\delta T_f^e$ , respectively, during cooling (blue line) and heating (orange line) at 10 °C/min for B<sub>2</sub>O<sub>3</sub>. (b) The simulated imaginary part of heat capacity ( $C_p$ ") of TMDSC (blue line) for PVAc and the Gaussian fit (orange line) following the DFDT method. (c) and (d)  $\delta T_f^e$  at the glass transition, and temperature fluctuation ( $\delta T$ ) calculated from the Gaussian fitting of simulated  $C_p$ ". Open circles in (d) represent the measured  $\delta T$  taken from Ref. 27, which were obtained by either fitting Gaussian to the measured  $C_p$ " or were estimated from the width of the glass transition measured by standard DSC. The detailed method and the reference to the measured  $\delta T$  shown here are in Ref. 27. The insets of (d) include B<sub>2</sub>O<sub>3</sub>.

the temperature was kept at  $T_{\rm a}$  for  $10^8$  s until the system was fully equilibrated. The simulated results are shown in Fig. 11. Figure 11(a) shows the evolution of  $\langle T_{\rm f,i} \rangle$  during cooling, and Fig. 11(c) shows those during isothermal annealing, where  $t_{\rm a}$  is the annealing time.

When the system was cooled at the fastest cooling rate,  $\langle T_{f,i} \rangle$  was frozen almost instantaneously at the initial temperature. As the cooling rate becomes slower,  $\langle T_{f,i} \rangle$  becomes lower. This is the generic behavior of the cooling dependence of enthalpy/volume in glass dynamics. However, the cooling rate dependence on  $\delta T_f$  is more complex, as shown in Fig. 11(b). At slow cooling rates, the

**TABLE III.** The parameters for TMDSC simulation.  $\theta_c$  is the cooling rate before modulated heating.  $\langle \theta_h \rangle$  is the underline heating rate during modulated heating. P is the period of oscillation, where s is seconds.  $A_T$  is the amplitude of oscillation.

$\theta_c$ (°C/min)	$\langle \theta_h \rangle$ (°C/min)	<i>P</i> (s)	$A_T$ (°C)
1	1	100	0.8

initial  $\delta T_f$  remains low, but it progressively increases with increasing cooling rates and can even become higher than the equilibrium state value  $\delta T_f^e$  (shown in the dashed black line) when a much faster cooling rate is used, such as 100 °C/s and 10<sup>6</sup> °C/s. When the system is quenched at these higher cooling rates,  $\delta T_f$  exhibits a complex nonmonotonic evolution during isothermal annealing, as shown in Fig. 11(d). From Fig. 11(d), we see that the nonmonotonic evolution only happens when the initial  $\delta T_{\rm f}$  after the cooling is larger than the minimum  $\delta T_{\rm f}$  during annealing. To visualize the probability distribution after slow and fast cooling, the histograms are calculated from  $W_i$  and  $T_{f,i}$  after cooling (see Fig. 12). In Fig. 12, the probability density distribution after the slowest cooling at 0.2 °C/s is shown in blue, and the one after the fastest cooling at 10<sup>6</sup> °C/s is shown in red. Clearly, the tail of the fast relaxation domain appears for the fast quenched system in red. In addition, for a slow quenched system, the fast relaxation domains have already relaxed toward a lower fictive temperature, which narrows the distribution. Therefore, after cooling, there are no fast relaxation domains that relax faster than the slow one, and that prevents the distribution from narrowing during isothermal annealing. In fact, the simulation of

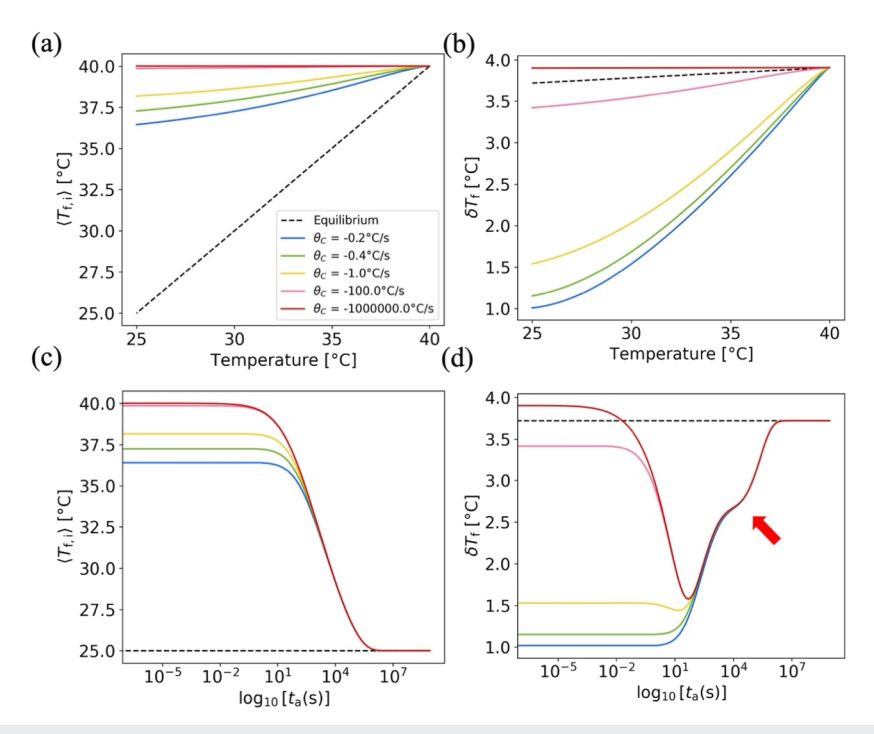


**FIG. 11.** (a) Evolution of average fictive temperature ( $\langle T_{t,i}^e \rangle$ ) during cooling at various rates from above  $T_g$  ( $T_0 = 40$  °C). The black dashed line represents the actual temperature. (b) The standard deviation of fictive temperature,  $\delta T_f$ , during cooling at various rates. The black dashed line represents the standard deviation of the equilibrium fictive temperature,  $\delta T_f^e$ . (c) Evolution of  $\langle T_f \rangle$  during isothermal annealing at 25 °C after cooling at various rates. The black dashed line is the average equilibrium fictive temperature,  $\langle T_{t,i}^e \rangle$ , which corresponds to the annealing temperature. (d) Evolution of  $\delta T_f$  during isothermal annealing at 25 °C after cooling at various rates. The red arrow points out the shoulder-like feature of  $\delta T_f$ . The black dashed line is  $\delta T_f^e$ . In (c) and (d),  $t_a$  indicates the annealing time.

Mauro *et al.* uses an infinitely fast quench rate, and the SAXS experiment performed by Mauro *et al.* also uses a fast quench rate from above  $T_{\rm g}$ .<sup>42</sup> These results suggest that one must use a high enough cooling rate to observe the nonmonotonic evolution of enthalpy/density fluctuations.

Qualitatively, the current model agrees well with the previous simulation of the enthalpy landscape model and the experimental result of the SAXS experiment. However, in comparison to the density fluctuation in Mauro et al.'s work,42 the current model predicts a narrower and smaller difference in  $\delta T_f^{\rm e}$  between before and after annealing. Currently, it is difficult to conclude whether this qualitative difference is a result of an artifact in the current model. This uncertainty arises due to the temperature dependence of  $\delta T_f^e$ , which is influenced by two factors: (1) the Vogel temperature as in Eq. (s4), and (2) the temperature dependence of  $\delta \ln \tau$  as shown in Eq. (s2) in the supplementary material. The first one illustrates that  $\delta T_f^e$  depends on fragility [see Eq. (24)]. The system with temperature-dependent  $\delta \ln \tau$  has weaker temperature dependence than  $\delta T_f^e$  as in Eq. (s4); however, if the system exhibits temperatureindependent  $\delta \ln \tau$ ,  $\delta T_{\rm f}^{\rm e}$  will have strong temperature dependence as in Eq. (s1) in the supplementary material. While the effects of fragility on the density fluctuation were rigorously investigated by Mauro using the enthalpy landscape model, 100 the contribution from temperature dependent nonexponentiality to the fluctuation has not been studied. Therefore, it would be necessary to investigate how the temperature dependence of nonexponentiality affects the density/enthalpy fluctuation during isothermal annealing below  $T_{\rm g}$  in both experiments and simulations.

The other qualitative difference between Fig. 11(d) and the results from the enthalpy landscape model is the shoulder like

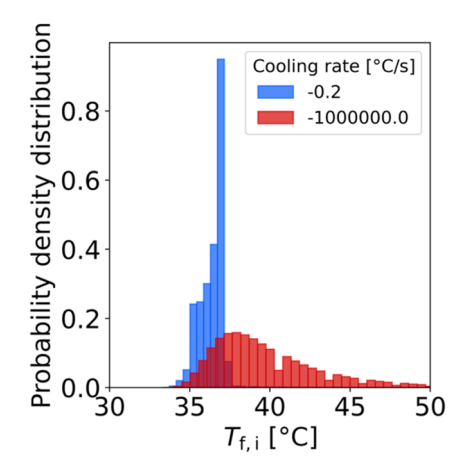


**FIG. 12.** The calculated histogram of probability distributions of  $T_{\rm f}$  after cooling at 0.2 °C/s in blue and 10<sup>6</sup> °C/s in red.

evolution after the minimum of  $\delta T_{\rm f}$  during isothermal annealing [indicated by the red arrow in Fig. 11(d)]. This shoulder is not observed in the results from the enthalpy-landscape model and its variant of the toy landscape model. This slowing down of the change in  $\delta T_{\rm f}$  can be explained as follows: (1) the fast relaxation domain reaches its local  $T_{\rm f,i}$ , which is comparable to that of the slow domains, and (2) the relaxation time of the initially fast domain becomes somewhat close to that of the slow domain. Consequently, both the fast and slow relaxation domains relax almost at the same rate, thus slowing down the change in  $\delta T_{\rm f}$ . We can avoid this situation by raising  $T_{\rm a}$ . Because the  $T_{\rm f,i}$  of the fast domain relaxes to its corresponding  $T_{\rm f,i}^{\rm e}$ , where such  $T_{\rm f,i}^{\rm e}$  is higher than the  $T_{\rm f,i}$  of the slow domain, only the slow domain relaxes toward a much lower  $T_{\rm f,i}^{\rm e}$  after the minimum of  $\delta T_{\rm f}$ . In Fig. s4(d) of the supplementary material, it is found that this shoulder vanishes when  $T_{\rm a}=30\,^{\circ}{\rm C}$ .

### IV. CONCLUSION

We have developed a phenomenological model that accounts for both temperature-dependent nonexponentiality and enthalpy fluctuation by incorporating the local equilibrium fictive temperature  $(T_{f,i}^e)$  in a heterogeneous system. The model was implemented for various organic and inorganic systems, and it was found that the calculated non-exponentiality factors  $\beta_{\mathrm{KWW}}$  show good agreement with previous experimental and simulation results. It is shown that the present model can predict both temperature-dependent nonexponentiality and enthalpy fluctuations for various thermal histories only by fitting normalized heat capacity curves around the glass transition. We demonstrate that the present model successfully predicts relaxation processes both near equilibrium and far from equilibrium. Near equilibrium, Kovacs' volume relaxation measurement on PVAc after temperature jumps is successfully simulated using the current model. Far from equilibrium, where the TNMH model fails, the volume relaxation data of Scherer<sup>47</sup> and the enthalpy relaxation measurements of Lancelotti et al.48 are successfully modeled with a single set of four parameters when multiple sets of parameters are required to describe the dynamics near and far from equilibrium with the TNM model. We emphasize that the number of fitting parameters used in our model is the same as that of the TNMH model and the KAHR model. Therefore, these results indicate that accounting for temperature dependent nonexponentiality in a model is necessary to describe the dynamics of glass relaxation far from equilibrium. Moreover, another advantage of the present model is its flexibility, which includes (1) allowing the implementation of any relaxation model to the present model if such model accounts for both equilibrium and nonequilibrium states, and (2) allowing the implementation of multiple distributions of relaxation time. The first one is similar to the traditional TNM model, where the traditional TNM model can implement both the TNM equation and the Adam-Gibbs equation depending on one's interest. If one wants to use the TNM model in the current framework, one may define the activation energy of relaxation time to have a distribution, just as the present model defines  $T_{\rm v}$  to have a distribution. The second one is the most unique aspect of the current model, which can implement any number of distributions of relaxation time. It has been known in the literature that some systems have two-step relaxation dynamics when subjected to long isothermal annealing far below  $T_{\rm g}$ . The present model would permit the implementation of two distributions with different assumptions (such as two distributions with different sets of model parameters) and predict how the enthalpy relaxation takes place under various thermal histories. This would permit us to check if the chosen assumptions are valid by comparing them with experiments. Therefore, the present model could serve as a test bed to study the contribution of structural heterogeneity to the macroscopic relaxation dynamics. Finally, the present model does not require computationally expensive resources, in contrast to other physics-motivated first principle models such as those in Refs. 41 and 57. Consequently, our model can expedite fundamental research aimed at a deeper understanding of how spatial heterogeneity contributes to the macroscopic relaxation dynamics. Additionally, it can be a powerful tool for industry if one wants to predict relaxation dynamics far from equilibrium, where temperature-dependent nonexponentiality significantly influences the relaxation dynamics.

#### SUPPLEMENTARY MATERIAL

The supplementary material provides (1) the detail derivations of Eq. (7), (2) the simulation results of the model using Gaussian distribution for  $Y_i$ , (3) the initial fractional deviation  $M_{\rm ini}$  of PVAc before annealing and the measured vs the simulated M(t) from the current model, the TNMH model with the TNM equation, and the TNMH model with the AG equation, (4) the simulation of fictive temperature fluctuation during isothermal annealing at different annealing temperature, and (5) a list of the values of  $X_i^{\rm ref}$  and  $\ln \tau_i/\tau_{\rm KWW}$  for each f.

### **ACKNOWLEDGMENTS**

The authors acknowledge financial support from NSF-DMR under Grant No. 1832817.

### **AUTHOR DECLARATIONS**

### **Conflict of Interest**

The authors have no conflicts to disclose.

### **Author Contributions**

**Wataru Takeda**: Conceptualization (equal); Methodology (equal); Validation (equal); Writing – original draft (equal). **Pierre Lucas**: Funding acquisition (equal); Supervision (equal); Writing – review & editing (equal).

#### **DATA AVAILABILITY**

The data that support the findings of this study are available from the corresponding author upon reasonable request.

#### **REFERENCES**

<sup>1</sup>M. Wuttig and N. Yamada, "Phase-change materials for rewriteable data storage," Nat. Mater. 6, 824 (2007).

<sup>2</sup>B. J. Eggleton, B. Luther-Davies, and K. Richardson, "Chalcogenide photonics," Nat. Photonics 5, 141 (2011).

- <sup>3</sup>S. Vyazovkin and I. Dranca, "Effect of physical aging on nucleation of amorphous indomethacin," J. Phys. Chem. B 111, 7283 (2007).
- <sup>4</sup>A. Shearer, M. Montazerian, and J. C. Mauro, "Modern definition of bioactive glasses and glass-ceramics," J. Non-Cryst. Solids **608**, 122228 (2023). <sup>5</sup>M. D. Ediger and P. Harrowell, "Perspective: Supercooled liquids and glasses,"
- J. Chem. Phys. 137, 080901 (2012).
- <sup>6</sup>L. Berthier and G. Biroli, "Theoretical perspective on the glass transition and amorphous materials," Rev. Mod. Phys. 83, 587 (2011).
- <sup>7</sup>G. B. McKenna, "Looking at the glass transition: Challenges of extreme time Scales and other interesting problems, rubber," Rubber Chem. Technol. 93, 79
- $^{\mathbf{8}}$  J. C. Dyre, "Colloquium: The glass transition and elastic models of glass-forming liquids," Rev. Mod. Phys. 78, 953 (2006).
- <sup>9</sup> A. Q. Tool and C. G. Eicitlin, "Variations caused in the heating curves of glass by heat treatment," J. Am. Ceram. Soc. 14, 276 (1931).
- <sup>10</sup>C. T. Moynihan et al., "Structural relaxation in vitreous materials," Ann. N. Y. Acad. Sci. 279, 15 (1976).
- <sup>11</sup>C. A. Angell, "Relaxation in liquids, polymers and plastic crystals—Strong/fragile patterns and problems," J. Non-Cryst. Solids 131-133, 13 (1991).
- <sup>12</sup>R. Kohlrausch, "Theorie Des Elektrischen Rückstandes in Der Leidener Flasche," Ann. Phys. 167, 179 (1854).
- <sup>13</sup>G. Williams and D. C. Watts, "Non-symmetrical dielectric relaxation behaviour arising from a simple empirical decay function," Trans. Faraday Soc. 66, 80 (1970).
- <sup>14</sup>M. D. Ediger, "Spatially heterogeneous dynamics in supercooled liquids," Annu. Rev. Phys. Chem. 51, 99 (2000).
- <sup>15</sup>K. A. Kirchner et al., "Beyond the average: Spatial and temporal fluctuations in oxide glass-forming systems," Chem. Rev. 123, 1774 (2023).
- <sup>16</sup>G. Adam and J. H. Gibbs, "On the temperature dependence of cooperative relaxation properties in glass-forming liquids," J. Chem. Phys. 43, 139 (1965).
- <sup>17</sup>K. Schmidt-Rohr and H. W. Spiess, "Nature of nonexponential loss of correlation above the glass transition investigated by multidimensional NMR," Phys. Rev. Lett. 66, 3020 (1991).
- <sup>18</sup>U. Tracht, M. Wilhelm, A. Heuer, H. Feng, K. Schmidt-Rohr, and H. W. Spiess, "Length scale of dynamic heterogeneities at the glass transition determined by multidimensional nuclear magnetic resonance," Phys. Rev. Lett. 81, 2727
- <sup>19</sup>E. V. Russell, N. E. Israeloff, L. E. Walther, and H. Alvarez Gomariz, "Nanometer scale dielectric fluctuations at the glass transition," Phys. Rev. Lett. 81, 1461 (1998).
- <sup>20</sup>E. Donth, "The size of cooperatively rearranging regions at the glass transition," J. Non-Cryst. Solids 53, 325 (1982).
- <sup>21</sup> A. Widmer-Cooper, P. Harrowell, and H. Fynewever, "How reproducible are dynamic heterogeneities in a supercooled liquid?," Phys. Rev. Lett. 93, 135701
- <sup>22</sup>S. Karmakar, C. Dasgupta, and S. Sastry, "Growing length and time scales in
- glass-forming liquids," Proc. Natl. Acad. Sci. U. S. A. **106**, 3675 (2009).

  <sup>23</sup> P. Zhang, J. J. Maldonis, Z. Liu, J. Schroers, and P. M. Voyles, "Spatially heterogeneous dynamics in a metallic glass forming liquid imaged by electron correlation microscopy," Nat. Commun. 9, 1129 (2018).
- <sup>24</sup>X. Xia and P. G. Wolynes, "Fragilities of liquids predicted from the random first order transition theory of glasses," Proc. Natl. Acad. Sci. U. S. A. 97, 2990
- <sup>25</sup> A. S. Keys, L. O. Hedges, J. P. Garrahan, S. C. Glotzer, and D. Chandler, "Excitations are localized and relaxation is hierarchical in glass-forming liquids," Phys. Rev. X 1, 021013 (2011).
- $^{\bf 26}\text{E.}$  Donth, "General derivation of the WLF equation from a fluctuation approach to the glass transition," Acta Polym. 30, 481 (1979).
- <sup>27</sup>E. Hempel, G. Hempel, A. Hensel, C. Schick, and E. Donth, "Characteristic length of dynamic glass transition near  $T_g$  for a wide assortment of glass-forming substances," J. Phys. Chem. B 104, 2460 (2000).
- <sup>28</sup>R. Böhmer *et al.*, "Nature of the non-exponential primary relaxation in structural glass-formers probed by dynamically selective experiments," J. Non-Cryst. Solids 235-237, 1 (1998).

- <sup>29</sup>P. B. Macedo and A. Napolitano, "Effects of a distribution of volume relaxation times in the annealing of Bsc glass," J. Res. Natl. Bur. Stand., Sect. A 71A, 231
- <sup>30</sup>S. R. Nagel and P. K. Dixon, "Relation between stretched-exponential relaxation and Vogel-Fulcher behavior above the glass transition," J. Chem. Phys. 90, 3885 (1989).
- <sup>31</sup>R. Böhmer, K. L. Ngai, C. A. Angell, and D. J. Plazek, "Nonexponential relaxations in strong and fragile glass formers," J. Chem. Phys. 99, 4201 (1993).
- 32 K. L. Ngai, "Temperature dependence of the stretched exponent in structural relaxation of fragile glass-forming molecular liquids," J. Non-Cryst. Solids 131-133, 80 (1991).
- $^{33}$ D. L. Sidebottom, "Generic  $\alpha$  relaxation in a strong GeO  $_2$  glass melt," Phys. Rev. E 107, L012602 (2023).
- <sup>34</sup>X. Xia and P. G. Wolynes, "Microscopic theory of heterogeneity and nonexponential relaxations in supercooled liquids," Phys. Rev. Lett. 86, 5526
- <sup>35</sup>A. Arbe, J. Colmenero, M. Monkenbusch, and D. Richter, "Dynamics of glassforming polymers: 'Homogeneous' versus 'heterogeneous' scenario," Phys. Rev. Lett. 81, 590 (1998).
- <sup>36</sup>R. Richert, "Homogeneous dispersion of dielectric responses in a simple glass," J. Non-Cryst. Solids 172-174, 209 (1994).
- <sup>37</sup>D. Diaz Vela and D. S. Simmons, "The microscopic origins of stretched exponential relaxation in two model glass-forming liquids as probed by simulations in the isoconfigurational ensemble," J. Chem. Phys. 153, 234503 (2020).
- 38 N. A. Bokov, "Light scattering studies of glasses in the glass transition region," J. Non-Cryst. Solids 177, 74 (1994).
- <sup>39</sup>C. T. Moynihan and J. Schroeder, "Non-exponential structural relaxation, anomalous light scattering and nanoscale inhomogeneities in glass-forming liquids," J. Non-Cryst. Solids 160, 52 (1993).
- <sup>40</sup>M. Lee, S. K. Saha, C. T. Moynihan, and J. Schroeder, "Non-exponential structural relaxation, anomalous light scattering and nanoscale inhomogeneities in glasses," J. Non-Cryst. Solids 222, 369 (1997).
- <sup>41</sup>J. C. Mauro and R. J. Loucks, "Selenium glass transition: A model based on the enthalpy landscape approach and nonequilibrium statistical mechanics," Phys. Rev. B 76, 174202 (2007).
- <sup>42</sup>J. C. Mauro, S. S. Uzun, W. Bras, and S. Sen, "Nonmonotonic evolution of density fluctuations during glass relaxation," Phys. Rev. Lett. 102, 155506 (2009).
- <sup>43</sup>O. S. Narayanaswamy, "A model of structural relaxation in glass," J. Am. Ceram. Soc. 54, 491 (1971).
- <sup>44</sup>I. M. Hodge and A. R. Berens, "Effects of annealing and prior history on enthalpy relaxation in glassy polymers. 2. Mathematical modeling," Macromolecules 15, 762 (1982).
- $^{\mathbf{45}}\mathrm{J}.$  M. Hutchinson and A. J. Kovacs, "A simple phenomenological approach to the thermal behavior of glasses during uniform heating or cooling," J. Polym. Sci.: Polym. Phys. Ed. 14, 1575 (1976).
- <sup>46</sup> A. J. Kovacs, J. J. Aklonis, J. M. Hutchinson, and A. R. Ramos, "Isobaric volume and enthalpy recovery of glasses. II. A transparent multiparameter theory," J. Polym. Sci., Part B: Polym. Phys. 34, 2467 (1996).
- <sup>47</sup>G. W. Scherer, "Volume relaxation far from equilibrium," J. Am. Ceram. Soc. 69, 374 (1986).
- $^{\mathbf{48}}$  R. F. Lancelotti, E. D. Zanotto, and S. Sen, "Kinetics of physical aging of a silicate glass following temperature up- and down-jumps," J. Chem. Phys. 160, 034504 (2024).
- <sup>49</sup>S. K. S. Mazinani and R. Richert, "Enthalpy recovery in glassy materials: Heterogeneous versus homogenous models," J. Chem. Phys. 136, 174515 (2012).
- <sup>50</sup>C. J. Wilkinson, Y. Z. Mauro, and J. C. Mauro, "RelaxPy: Python code for modeling of glass relaxation behavior," SoftwareX 7, 255 (2018).
- <sup>51</sup>R. Richert, "Heat capacity in the glass transition range modeled on the basis of heterogeneous dynamics," J. Chem. Phys. 134, 144501 (2011).
- $^{\bf 52}{\rm C.~J.}$  Wilkinson, K.-H. Lee, D. Yin, and J. C. Mauro, "Modeling the relaxation of fluctuations in glass during the Ritland crossover experiment," MRS Commun. 12, 1060 (2022).
- <sup>53</sup>D. Cangialosi, A. Alegría, and J. Colmenero, "On the temperature dependence of the nonexponentiality in glass-forming liquids," J. Chem. Phys. 130, 124902 (2009).

- <sup>54</sup>H. Huth, M. Beiner, and E. Donth, "Temperature dependence of glass-transition cooperativity from heat-capacity spectroscopy: Two post-Adam-Gibbs variants," Phys. Rev. B **61**, 15092 (2000).
- $^{55}$ O. Gulbiten, J. C. Mauro, and P. Lucas, "Relaxation of enthalpy fluctuations during sub-T $_{\rm g}$  annealing of glassy selenium," J. Chem. Phys. 138, 244504 (2013).
- <sup>56</sup>J. E. K. Schawe, "Vitrification in a wide cooling rate range: The relations between cooling rate, relaxation time, transition width, and fragility," J. Chem. Phys. 141, 184905 (2014).
- <sup>57</sup> A. Wisitsorasak and P. G. Wolynes, "Dynamical heterogeneity of the glassy state," J. Phys. Chem. B 118, 7835 (2014).
- <sup>58</sup>C. P. Lindsey and G. D. Patterson, "Detailed comparison of the Williams–Watts and Cole–Davidson functions," J. Chem. Phys. **73**, 3348 (1980).
- <sup>59</sup>S. Havriliak and S. Negami, "A complex plane representation of dielectric and mechanical relaxation processes in some polymers," <u>Polymer 8</u>, 161 (1967).
- <sup>60</sup>R. Richert and M. Richert, "Dynamic heterogeneity, spatially distributed stretched-exponential patterns, and transient dispersions in solvation dynamics," Phys. Rev. E **58**, 779 (1998).
- <sup>61</sup> R. Richert, "Heterogeneous dynamics in liquids: Fluctuations in space and time," J. Phys.: Condens. Matter 14, R703 (2002).
- <sup>62</sup> X. Guo, J. C. Mauro, D. C. Allan, and M. M. Smedskjaer, "Predictive model for the composition dependence of glassy dynamics," J. Am. Ceram. Soc. **101**, 1169 (2018).
- <sup>63</sup>I. M. Hodge, "Adam-Gibbs formulation of nonlinearity in glassy-state relaxations," <u>Macromolecules</u> 19, 936 (1986).
- <sup>64</sup>P. Virtanen *et al.*, "SciPy 1.0: Fundamental algorithms for scientific computing in Python," Nat. Methods 17, 261 (2020).
- <sup>65</sup>J. Málek, R. Svoboda, P. Pustková, and P. Čičmanec, "Volume and enthalpy relaxation of a-Se in the glass transition region," J. Non-Cryst. Solids 355, 264 (2009).
- <sup>66</sup> M. A. Debolt, A. J. Easteal, P. B. Macedo, and C. T. Moynihan, "Analysis of structural relaxation in glass using rate heating data," J. Am. Ceram. Soc. **59**, 16 (1976).
- <sup>67</sup> H. Sasabe and C. T. Moynihan, "Structural relaxation in poly(vinyl acetate)," J. Polym. Sci.: Polym. Phys. Ed. 16, 1447 (1978).
- <sup>68</sup>V. Velikov, S. Borick, and C. A. Angell, "The glass transition of water, based on hyperquenching experiments," Science **294**, 2335 (2001).
- <sup>69</sup>L. M. Wang, V. Velikov, and C. A. Angell, "Direct determination of kinetic fragility indices of glassforming liquids by differential scanning calorimetry: Kinetic versus thermodynamic fragilities," J. Chem. Phys. 117, 10184 (2002).
- $^{70}\mathrm{C}.$  Gao and H. M. Ma, "Enthalpy relaxation in D-sorbitol glass," J. Therm. Anal. Calorim. 120, 1905 (2015).
- <sup>71</sup> C. M. Roland, P. G. Santangelo, D. J. Plazek, and K. M. Bernatz, "Creep of selenium near the glass temperature," J. Chem. Phys. 111, 9337 (1999).
- <sup>72</sup>G. D. Chryssikos, J. A. Duffy, J. M. Hutchinson, M. D. Ingram, E. I. Kamitsos, and A. J. Pappin, "Lithium borate glasses: A quantitative study of strength and fragility," J. Non-Cryst. Solids 172–174, 378 (1994).
- <sup>73</sup>P. K. Dixon and S. R. Nagel, "Frequency-dependent specific heat and thermal conductivity at the glass transition in *o*-terphenyl mixtures," Phys. Rev. Lett. **61**, 341 (1988).
- <sup>74</sup>N. O. Birge and S. R. Nagel, "Specific-heat spectroscopy of the glass transition," Phys. Rev. Lett. **54**, 2674 (1985).
- <sup>75</sup> K. J. Crowley and G. Zografi, "The use of thermal methods for predicting glass-former fragility," Thermochim. Acta 380, 79 (2001).
- <sup>76</sup>M. Naoki, H. Endou, and K. Matsumoto, "Pressure effects on dielectric relaxation of supercooled ortho-terphenyl," J. Phys. Chem. 91, 4169 (1987).
- <sup>77</sup>J. Zhao and G. B. McKenna, "Temperature divergence of the dynamics of a poly(vinyl acetate) glass: Dielectric vs. Mechanical behaviors," J. Chem. Phys. 136, 154901 (2012).
- <sup>78</sup>U. Schneider, P. Lunkenheimer, R. Brand, and A. Loidl, "Dielectric and far-infrared spectroscopy of glycerol," J. Non-Cryst. Solids 235–237, 173 (1998).

- <sup>79</sup>X. H. Qiu and M. D. Ediger, "Length scale of dynamic heterogeneity in supercooled D-sorbitol: Comparison to model predictions," J. Phys. Chem. B **107**, 459 (2003).
- <sup>80</sup>R. Böhmer and C. A. Angell, "Elastic and viscoelastic properties of amorphous selenium and identification of the phase transition between ring and chain structures," Phys. Rev. B 48, 5857 (1993).
- <sup>81</sup> V. Lubchenko and P. G. Wolynes, "Theory of aging in structural glasses," J. Chem. Phys. 121, 2852 (2004).
- <sup>82</sup> M. P. Eastwood, T. Chitra, J. M. Jumper, K. Palmo, A. C. Pan, and D. E. Shaw, "Rotational relaxation in *ortho*-terphenyl: Using atomistic simulations to bridge theory and experiment," J. Phys. Chem. B 117, 12898 (2013).
- <sup>83</sup> B. Jakobsen, T. Hecksher, T. Christensen, N. B. Olsen, J. C. Dyre, and K. Niss, "Communication: Identical temperature dependence of the time scales of several linear-response functions of two glass-forming liquids," J. Chem. Phys. 136, 081102 (2012).
- <sup>84</sup>R. Richert, "On the dielectric susceptibility spectra of supercooled o-terphenyl," J. Chem. Phys. **123**, 10 (2005).
- <sup>85</sup>R. Richert and H. Wagner, "The dielectric modulus: Relaxation versus retardation," Solid State Ionics 105, 167 (1998).
- <sup>86</sup>D. Sidebottom, R. Bergman, L. Börjesson, and L. M. Torell, "Two-step relaxation decay in a strong glass former," Phys. Rev. Lett. **71**, 2260 (1993).
- <sup>87</sup>G. M. Bartenev and V. A. Lomovskoi, "Relaxation time spectra and the peculiarities of the process of boron anhydride glass transition," J. Non-Cryst. Solids 146, 225 (1992).
- $^{88}$  A. Schönhals, F. Kremer, A. Hofmann, and E. W. Fischer, "Anomalies in the scaling of the  $\alpha$ -relaxation studied by dielectric spectroscopy," Physica A  $201,\,263$  (1993).
- <sup>89</sup>J. Málek, "Structural relaxation rate and aging in amorphous solids," J. Phys. Chem. C 127, 6080 (2023).
- <sup>90</sup> A. J. Kovacs, "Transition Vitreuse Dans Les Polymères Amorphes. Etude Phénoménologique," Fortschr. Hochpolym.-Forsch. 3, 394 (1964).
- <sup>91</sup> J. E. McKinney and M. Goldstein, "PVT relationships for liquid and glassy poly(vinyl acetate)," J. Res. Natl. Bur. Stand., Sect. A 78A, 331 (1974).
- <sup>52</sup> R. Svoboda, P. Pustková, and J. Málek, "Structural relaxation of polyvinyl acetate (PVAc)," Polymer **49**, 3176 (2008).
- <sup>93</sup>C. T. Moynihan, A. J. Easteal, M. A. De Bolt, and J. Tucker, "Dependence of the fictive temperature of glass on cooling rate," J. Am. Ceram. Soc. **59**, 12
- <sup>94</sup>S. Hara and M. Suetoshi, Density change of glass in transformation range, Reports Res. Lab., Asahi Glass Co., Ltd., Vol. 5, p. 126, 1955.
- <sup>95</sup>J. M. Hutchinson and S. Montserrat, "A theoretical model of temperature-modulated differential scanning calorimetry in the glass transition region," Thermochim. Acta **304–305**, 257 (1997).
- <sup>96</sup>S. Weyer, M. Merzlyakov, and C. Schick, "Application of an extended Tool-Narayanaswamy-Moynihan model," Thermochim. Acta 377, 85 (2001).
- <sup>97</sup>B. Wunderlich, A. Boller, I. Okazaki, and K. Ishikiriyama, "Heat-capacity determination by temperature-modulated DSC and its separation from transition effects," Thermochim. Acta **304–305**, 125 (1997).
- <sup>98</sup> A. Hensel and C. Schick, "Relation between freezing-in due to linear cooling and the dynamic glass transition temperature by temperature-modulated DSC," J. Non-Cryst. Solids 235–237, 510 (1998).
- <sup>99</sup>E. Donth, "Characteristic length of the glass transition," J. Polym. Sci., Part B: Polym. Phys. 34, 2881 (1996).
- <sup>100</sup>J. C. Mauro, "Effect of fragility on relaxation of density fluctuations in glass," J. Non-Cryst. Solids 357, 3520 (2011).
- <sup>101</sup>D. Cangialosi, V. M. Boucher, A. Alegría, and J. Colmenero, "Direct evidence of two equilibration mechanisms in glassy polymers," Phys. Rev. Lett. **111**, 095701 (2013)
- <sup>102</sup> A. Morvan, N. Delpouve, A. Vella, and A. Saiter-Fourcin, "Physical aging of selenium glass: Assessing the double mechanism of equilibration and the crystallization process," J. Non-Cryst. Solids **570**, 121013 (2021).